UNCLASSIFIED

[redacted]

Copy 49

NASA TM X-18

NASA TM X-18

TECHNICAL MEMORANDUM

X - 18

AN EXPERIMENTAL AND ANALYTICAL INVESTIGATION OF THE DYNAMICS OF TWO BLUNT BODIES AT SUBSONIC SPEEDS

By Donald A. Buell and Norman S. Johnson

Ames Research Center
Moffett Field, Calif.

CLASSIFICATION CHANGED TO UNCLASSIFIED
BY AUTHORITY OF NASA CLASSIFICATION CHANGE
NOTICES, CHANGE NO. 209-23, EFF. 12/19/70 gm

CLASSIFIED DOCUMENT - TITLE UNCLASSIFIED

This material contains information affecting the national defense of the United States within the meaning of the espionage laws, Title 18, U.S.C., Secs. 793 and 794, the transmission or revelation of which in any manner to an unauthorized person is prohibited by law.

NATIONAL AERONAUTICS AND SPACE ADMINISTRATION

WASHINGTON August 1959

[redacted]

UNCLASSIFIED

8341

NATIONAL AERONAUTICS AND SPACE ADMINISTRATION

TECHNICAL MEMORANDUM X-18

AN EXPERIMENTAL AND ANALYTICAL INVESTIGATION OF THE DYNAMICS OF TWO BLUNT BODIES AT SUBSONIC SPEEDS*

By Donald A. Buell and Norman S. Johnson

SUMMARY

An experimental and analog-computer study has been conducted of the dynamics of two blunt bodies at subsonic speeds. Two forebody shapes were considered; one was a paraboloid, and the other was a blunted cone with a nose radius equal to the maximum diameter. Both bodies had afterbodies with maximum diameters less than those of the forebodies. Wind-tunnel tests of models of the bodies and their components were made to establish static-stability characteristics at angles of attack up to 72°, damping derivatives up to 18°, and pressure coefficients at the base of the forebodies up to 40°. A free fall from an altitude of 35,700 feet provided data on the actual trajectory and velocities of one body and gave qualitative information about its damping characteristics.

The analog-computer study was made to determine the trajectories and dynamic stability of representative bodies which have entered the subsonic portion of their flight at various attitudes and altitudes. The results showed that the bodies were dynamically stable for most of the conditions considered. Limitations in the wind-tunnel data left doubt as to the stability of the bodies at large angles of oscillation. The computer results closely checked the information available on flights of the free-fall models.

INTRODUCTION

The advantages of bluntness for vehicles entering the atmosphere at hypersonic speeds are well known. Blunt-nosed bodies of low fineness ratio are particularly suitable for such vehicles if problems associated with high temperatures are to be minimized. However, reference 1, among others, has pointed out the possibility of dynamic instability for such shapes in the low-altitude portion of a ballistic trajectory. A typical

*Title, Unclassified

[redacted]

blunt-nosed vehicle would have a subsonic flight velocity in this portion of the trajectory. An investigation, therefore, was undertaken to establish the dynamics of two representative models at subsonic speeds. This investigation was carried out in three parts: tests in the Ames 12-foot pressure wind tunnel to evaluate the aerodynamic characteristics, computer studies utilizing the wind-tunnel data to predict the behavior of such missiles in a ballistic trajectory, and free-fall tests to check the validity of the simulations.

Tests of similar models at supersonic speeds are reported in references 2 and 3. The results of these tests have indicated the possibility of at least a small oscillation as the vehicle decelerates through supersonic speeds.

NOMENCLATURE

C_D drag coefficient, $\dfrac{\text{drag}}{(1/2)\rho V^2 S}$

C_L lift coefficient, $\dfrac{\text{lift}}{(1/2)\rho V^2 S}$

C_m pitching-moment coefficient, $\dfrac{\text{pitching moment}}{(1/2)\rho V^2 SD}$

(Moment center is 0.69 L behind nose for paraboloid and 0.82 L behind nose for blunted cone unless otherwise noted.)

$C_{m_q} + C_{m_{\dot\alpha}}$ damping coefficient, $\dfrac{\partial C_m}{\partial(qD/V)} + \dfrac{\partial C_m}{\partial(\dot\alpha D/V)}$

C_p base-pressure coefficient, $\dfrac{(\text{base pressure}) - (\text{free-stream static pressure})}{(1/2)\rho V^2}$

c.g. center of gravity

D maximum diameter

F moment due to bearing resistance

f frequency of oscillation

g acceleration due to gravity (32.2 ft/sec^2)

[redacted]

h	altitude above sea level
K	aerodynamic "spring" constant, $-C_{m_\alpha} \frac{1}{2} \rho V^2 SD$
I	mass moment of inertia, $m\sigma^2$
L	length of forebody
M	Mach number of body along flight path
m	mass
P	damping moment
q	pitching velocity
R	free-stream Reynolds number based on D
S	frontal area, $\frac{\pi D^2}{4}$
$T_{1/2}$	time to damp to one-half amplitude
T_2	time to double amplitude
t	time
V	velocity of body along flight path with respect to air mass
V_E	velocity of body along flight path with respect to earth
V_{wind}	wind velocity
x	horizontal range coordinate
x_m	axial coordinate of forebody
y_m	radial coordinate of forebody
α	angle of attack, radians except where otherwise noted
γ	angle of flight path above horizontal
ω	circular frequency of oscillation, $2\pi f$

[redacted]

ρ air density

σ radius of gyration

$(\dot{\ })$ derivative with respect to time

Subscripts

e envelope value

f forebody

o initial reference value

YY about Y axis, which is perpendicular to longitudinal axis

MODELS AND APPARATUS

Wind Tunnel

Three bodies of revolution were tested in the wind tunnel. One model had a parabolic forebody with a maximum frontal area of 2.011 square feet. The other two models were similar bodies with highly blunted conical noses. The maximum frontal area of one blunted-cone model was equal to that of the paraboloid, while the second blunted-cone model had a frontal area of 0.159 square feet. Dimensions of the models are given in figure 1(a), and one model is shown mounted in the wind tunnel in figure 1(b). The center of moments and of rotation was located in most cases 0.69 of the forebody length behind the nose of the paraboloid and 0.82 of the forebody length behind the nose of the blunted-cone models. The exceptions to these locations are noted in the results.

The two larger models had separate forebody and afterbody shells made of Fiberglas and plastic attached to aluminum skeletons. The afterbody shell was removable in each case. The smaller model was of one-piece construction and was made of aluminum.

For static-force tests the larger models were mounted on a strain-gage balance enclosed by the model and supported by a 4-inch-diameter sting. The smaller model was mounted on a strain-gage balance which was enclosed partly within the model and partly within the sting.

To measure damping characteristics, the larger models were installed on crossed flexure pivots enclosed by the model and supported by a

[redacted]

2-1/4-inch-diameter sting. The flexure pivots were arranged to permit pitch oscillations of the model about the center of moments. No attempt was made to locate the center of gravity of the model at the center of moments, but previous tests have indicated that little error was incurred by this procedure. Pitch oscillations were excited and maintained by an electromagnetic shaker remote from the model but connected to it by a push rod through the sting. The shaker was in turn excited by an electronic feedback network which caused the model to oscillate at the desired amplitude at the natural frequency of the system. The amplitude and phase relationship of the damping moments and deflections were evaluated in an analog computing system connected to strain gages on the push rod and flexures. Reference 4 describes the equipment in more detail.

Finally, the larger models were sting mounted on a set of ball-bearing gimbals, leaving the model free to pitch and yaw. Initial displacements in pitch were achieved by a pneumatically operated push rod which engaged the base of the model. In these tests the model center of gravity and center of rotation were made to correspond to the center of moments previously defined.

Free Fall

The dimensions of the models which were dropped in free-fall tests are shown in figure 2(a) and one is pictured in figure 2(b) mounted on the drop aircraft. Other geometric and mass data are given in table I. These models were constructed of wood and lead so as to have center-of-gravity positions the same as the center of moments of the wind-tunnel models. The mass per unit of frontal area of the models was intended to be typical of full-scale vehicles so that decelerations would be properly simulated. An analysis similar to that in reference 1 shows that the rate of damping an oscillation is a function of the ratio of the reference length, D, to radius of gyration, σ, as well as the mass per unit of frontal area. Therefore, representative values of the ratio D/σ were selected for the models so that full-scale damping rates would be simulated. Since the frequency of oscillation is not solely a function of these particular ratios, the model frequencies and reduced frequencies were not typical of full-scale values.

TEST PROCEDURES AND DATA REDUCTION

Wind-Tunnel Static-Force Tests

In the first series of wind-tunnel tests, static force and moment measurements were made, covering three different angle-of-attack ranges.

Successive ranges were attained by mounting the model on stings bent to the necessary angle. These ranges were: (1) -4° to 24° (for all three models), (2) 14° to 40° (larger models), and (3) 48° to 72° (smaller model). In the lower angle-of-attack range the larger models were tested with and without afterbody shells (although the aluminum tube shown by dashed lines in figure 1(a) was not removed). In tests with the afterbodies, both average and instantaneous values of the pressure on the forebody base just outboard of the afterbody were measured. The average values were obtained by connections to a liquid manometer, and the time dependent values were measured with inductance-type pressure cells. The Reynolds number for these static-stability and pressure tests varied from 0.45 million to 5.3 million, and the Mach number was varied from 0.38 to 0.94.

During the investigation some question arose as to the validity of the data at the highest Mach numbers. In the initial tests the larger models exhibited an abrupt increase in drag and a decrease in base pressure as the Mach number was increased above 0.80. In succeeding tests the small model displayed similar characteristics at Mach numbers above 0.90. It was concluded from the data and from wall pressure measurements that the tunnel flow was being choked by the model wake at these speeds, and the data were discarded. It is of interest to note that calculation of the choking Mach number from a consideration of the solid blockage of the model would be almost 0.06 higher than the values arrived at experimentally.

Corrections calculated by the method of reference 5 were applied to the data for the larger models to take into account the effects of constriction by the wind-tunnel walls. This correction amounted to about 2 percent of the Mach number and dynamic pressure and 1/2 percent of the drag at a Mach number of 0.80.

It was presumed that the results would be most nearly representative of a typical vehicle if the base pressure were not adjusted to the free-stream static pressure, as is the usual practice with sting-mounted models. No corrections were made to account for the effects of sting interference. However, the base pressures were measured and representative values will be shown.

Wind-Tunnel Oscillation Tests

Oscillation tests were performed in the wind tunnel on the shaker apparatus using the larger models. Data were taken with the models oscillating at several selected amplitudes for various angles of attack. The angle of attack for these tests was varied from -10° to 18° but was often limited by excessive bending of the flexure-pivot support due to the static pitching moments on the model. The models were tested with and without afterbody shells and with and without internal weights, which were situated so as to permit a change of frequency of oscillation from about 10 to 7-1/2 cycles per second. For some tests the center of rotation (and moments) was changed to more rearward positions approaching that for static instability. Reynolds number was varied from 1.5 million to 3.0 million, and Mach number was varied from 0.38 to 0.80 in these oscillation tests.

The internal damping of the shaker apparatus and of the models was determined by oscillating the models, wind off, at various tunnel pressures and extrapolating the values to zero pressure. These values of internal damping, which were equivalent to a $C_{m_q} + C_{m_{\dot{\alpha}}}$ of the order of -0.05, were subtracted from the measured damping.

Additional oscillation tests were performed with the larger models on gimbals at a Reynolds number of 1.5 million and Mach numbers of 0.60 to 0.80 with and without afterbodies. In these tests, removal of the afterbody included removal of the aluminum tube behind the forebody. The procedure followed was to give the model a pitch disturbance (6-1/2° with afterbodies on and at least 15° with afterbodies off) and allow it to damp to the steady-state oscillation. Movies were made of the model pitching and yawing motions at about 24 frames per second during the decay of the pitch disturbance.

In the reduction of data from the gimbals tests it was assumed that the recorded motion was approximately described by the equation

$$I\ddot{\alpha} + P\dot{\alpha} + K\alpha = 0$$

(Little change in yawing amplitude was observed during the changes in pitching amplitude.) The damping term P included both aerodynamic damping and bearing damping with the approximation stated in reference 6 that

$$P_{bearing} = \frac{4F}{\pi\omega\alpha_e}$$

where $F = 0.0015 \times \text{drag} \times \text{bearing radius}$. The latter relation represents the resistance to movement of a good ball bearing supporting the drag load. The spring constant K was calculated from the static-moment data. From the movies of the motion it was possible to determine roughly the envelope values of angle of oscillation, α_e, which is related to the damping in the solution of the equation of motion by

$$\alpha_e = \alpha_o e^{-(P/2I)(t-t_o)}$$

It was then possible to calculate the aerodynamic damping coefficients, knowing that

$$P = P_{bearing} - (C_{m_q} + C_{m_{\dot{\alpha}}}) \frac{1}{2} \rho VSD^2$$

Average values were determined for ranges of α_e from maximum to one-half amplitude and from about 6-1/2° to 3-1/2°. The estimated bearing damping was very small in these ranges, compared to the aerodynamic damping.

Flight Tests

In the free-fall tests the models were released at 40,000 feet altitude at a Mach number of 0.80. In most cases, pitch, yaw, and roll disturbances were imparted to the model on release from the aircraft. The motion of the models was recorded by cameras in the drop airplane, in accompanying aircraft, and on the ground. Timing of the records depended upon the frame speed of the cameras. The trajectory of one of the drops was determined by the use of Askania phototheodolites.

Computer Study

A computer study was made with an electronic simulation of the motion of the models in the free-fall tests and also in various other ballistic trajectories. Inputs to the simulator were varied to indicate the influence of certain variables on the subsonic dynamic stability characteristics of the models. Variations in the initial flight-path angle and altitude at which the flight velocity became subsonic were included in the study.

The geometric and mass characteristics used in the simulation were those of the flight-test models and are given in table I. The aerodynamic characteristics as evaluated in the wind-tunnel tests were used in the simulation unless otherwise noted. Since no measurement of $C_{m_{\dot{\alpha}}}$ was made separately, it was assumed equal to zero, and C_{m_q} was assumed equal to the measured value of $C_{m_q} + C_{m_{\dot{\alpha}}}$.

Because of the symmetry of the models only three longitudinal equations of motion and certain additional equations were required in the simulation to determine the two-dimensional trajectory and the dynamic characteristics of the bodies. These equations follow:

$$\dot{\alpha} = q - \frac{C_L(\rho/2)SV}{m} + \frac{g}{V}\cos\gamma$$

$$\dot{q} = \frac{C_m(\rho/2)SV^2D}{I_{YY}} + C_{m_q}\frac{(\rho/2)SVD^2}{I_{YY}}q$$

$$\dot{V} = -C_D\frac{(\rho/2)SV^2}{m} - g\sin\gamma$$

$$\dot{h} = V\sin\gamma$$

$$\dot{x} = V\cos\gamma - V_{wind}$$

$$V_E = \sqrt{\dot{x}^2 + \dot{h}^2}$$

The simulation used the density-altitude relationship defined by the International Civil Aviation Organization.

RESULTS AND DISCUSSION

The results of the investigation fall into two groups: (1) the aerodynamic characteristics of the models determined in the wind tunnel, and (2) the computed dynamic response of models geometrically similar to the wind-tunnel models, as evaluated with the electronic simulator. The actual motion of free-fall models, which were the simulated models, is compared to the computed motion where possible.

Wind-Tunnel Measurements

Static force and moment characteristics.- The results of static-force tests of the large models at Reynolds numbers of 3 million or more are shown in figure 3. At low angles of attack the variation of drag coefficient with angle of attack (fig. 3(a)) approximates a cosine variation which is the variation followed by the frontal area projected normal to the free stream. The drag curves of the paraboloid depart from the cosine variation at about 30°, the angle of attack near which the forebody surface became tangent to the free-stream direction. However, the blunted-cone data depart from the cosine variation at much lower angles of attack, presumably because of flow separation near the intersection of the nose radius with the cone. This flow separation also was probably the main source of differences in lift and pitching-moment characteristics (figs. 3(b) and 3(c)) between the paraboloid and the blunted cone. The result was that the favorable lift and near-linear pitching-moment characteristics of the paraboloid were not realized on the blunted-cone model.

Removal of the afterbodies slightly decreased the drag of both models and also increased the lift at positive angles of attack but had no effect on the pitching moments. These results are similar to what would be expected from an increase in the fineness ratio of the forebody. Thus the main action of the afterbody appeared to be a spreading of the wake behind the forebody, increasing the effective diameter of the forebody.

It was convenient to extend the angle-of-attack range of the blunted-cone model to 72° by use of the smaller model. These data are presented in figure 4 and compared to those of figure 3 for the larger body (the dashed curves) to show the effect of Reynolds number. It should be noted that fairings of the data for the small model have been continued from an angle of attack of 24° to 48° although there were no data between these angles. At the maximum angle reached the drag coefficients were still large, the lift coefficients were small or negative, and the models were statically stable.

Damping coefficients for small angles of oscillation.- The damping in pitch of the large models was measured with the shaker apparatus which permitted a variation in the amplitude of oscillation and also in the angle of attack about which the oscillation occurred. A large oscillation about an angle of attack of 0° was considered to be the type of motion of most interest in the present investigation. It was presumed, as in a linear system, that measurements of damping for small oscillations over a wide angle-of-attack range would give representative data for the motion of interest. Actually, the measured damping almost always had a negative or very small positive value at angles of oscillation less than $\pm 1^{\circ}$ at any angle of attack. As the magnitude of oscillation was increased, the damping increased for most test conditions. As a consequence, the shaker measurements are only an approximation to the desired information. The measured damping for the smallest oscillation amplitudes are not presented since the accuracy of the instrumentation and the repeatability of the data were poor. The measured damping of the models when oscillating at the maximum available angle, $\pm 2^{\circ}$, about the nominal angle of attack is presented in figure 5.

The pitch damping of the models was positive for all the test conditions noted in figure 5(a). There were no effects of increasing the Reynolds number from 1.5 million to 3 million, within the accuracy of the data, and the effects of increasing the frequency of the oscillation from about 7 to 10 cps were small. The damping was greater without the afterbodies; however, there is some indication that the effects of the afterbodies were less at the higher angles of attack.

With more rearward center-of-gravity positions it was possible to obtain the damping characteristics of the models at higher angles of attack. These results are shown in figure 5(b) and are compared with data for the models from figure 5(a). There does not appear to be any easily defined trend of damping variation with angle of attack and center-of-gravity location. Only at angles of attack near 0 was the damping negative, and this occurred on the blunted-cone model with the most rearward center of gravity tested.

Damping coefficients for larger angles of oscillation.- The limitations on angle of oscillation imposed by the shaker apparatus were partially circumvented by the tests with the models mounted on ball-bearing gimbals. The results of these tests are shown in figure 6. Since the models oscillated about 0° angle of attack, the angles of attack noted in figure 6 represent the average peak angles of oscillation over the time history analyzed. The data are compared to average values of $C_{m_q} + C_{m_{\dot{\alpha}}}$ from the shaker data (faired lines) for angles of attack of 0° to 4°, a range available at all Mach numbers. The data with the model on gimbals have the same general level as the shaker data, regardless of angle of oscillation. The one exception to the agreement is the blunted cone with afterbody which has consistently higher damping on the gimbals than on the shaker. It is concluded that the shaker data are representative for these larger angles of oscillation.

Base-pressure measurements.- Coefficients of the pressures measured at the base of the models are shown in figure 7. The variation of the coefficients with angle of attack was less than 0.2 in the angle range investigated. Little significance is attached to the differences in pressure between models since the bases were somewhat different in shape. Discontinuities in the curves reflect the changes in the sting configuration, but the effect is small in terms of the forces on the model. The pressures in the region of separated flow behind the model might be of interest for reference or instrumentation purposes. Coefficients of the pressures measured on the base of the forebody for static conditions are presented in figure 8. The data show that pressure coefficients in this region are not greatly affected by angle of attack. At these Mach numbers the coefficients fell within ±0.1 of -0.4 at most angles of attack up to 40°. Pressures were also measured at other radial positions than those designated in figure 8 but merely showed a gradual progression in pressure from top to bottom. The variation of these base pressures with time at 0° angle of attack was also measured to explore the possibility of a predominant frequency of the pressure fluctuations. The presence of such a frequency near the natural frequency of a body could alter its damping characteristics. A frequency analysis of the measured pressures showed that many frequencies were present. However, the magnitude of the fluctuations generally decreased with increasing frequency. Typical values of the average pressure fluctuation analyzed with a band width of 1 cps ranged from 1/2 percent of the free-stream dynamic pressure at frequencies near 0 to 1/20 percent at a frequency of 50 cps.

Electronic Simulator Results

The free-fall tests of the two missile shapes were undertaken to provide a check of the applicability of the electronic simulation techniques. The only well-documented data obtained in the free-fall tests were a trajectory for the blunted cone from theodolite measurements and a short history of the changes in attitude of the blunted cone as recorded by the camera in the accompanying aircraft.

Figures 9 and 10 show a comparison between the trajectories of the actual and simulated flights for the blunted cone. This body was launched in level flight at $M = 0.8$ and an altitude of 40,000 feet. Ground camera data were available from the time the body reached an altitude of 35,700 feet and a flight-path angle of -44.6°. A wind velocity of about 47 feet per second was included so that the simulated trajectory would match the flight trajectory. The value agreed closely with the average prevailing wind in the vicinity on the day of the flight. The actual flight velocity (fig. 10) was obtained by differentiation of the theodolite measured flight trajectory and is referred to as V_E.

It was observed that the blunted cone had a large initial oscillation in angle of attack which for the simulation was assumed to be $\pm 32^{\circ}$. The simulation showed that the magnitude of the oscillation decreased from 32° to 16° in approximately 20 seconds and that the frequency increased from about 1.5 to 1.8 cps as the altitude decreased. The initial frequency of the oscillation was checked by flight records to within 5 percent. Visual observations by the tracking pilots ascertained that the oscillations did actually decrease during the flight for both configurations. The simulation technique appeared to be satisfactory on the basis of these comparisons with the available data.

The primary aim of the simulation was to determine the effects of pertinent variables on the dynamic stability of blunt missiles flying at a subsonic speed. The investigation was not limited to a specific trajectory. The intention was, rather, to make the results applicable to the subsonic portion of any trajectory which might possibly be anticipated. Consequently, consideration was given to a wide range of initial attitudes, altitudes, and flight-path angles. In the simulation the missile was "launched" at a subsonic speed. The conditions prevailing at this speed are termed "initial" conditions although they may be thought of more realistically as the continuation of a preceding flight history.

The relations developed in reference 1 between missile characteristics and response are quite useful in a qualitative interpretation of the simulator results. The dynamic stability is shown in reference 1 to be approximately a function of the entry angle, the altitude, the physical characteristics of the missile, and the factor

$$C_D - C_{L_\alpha} + (C_{m_q} + C_{m_{\dot{\alpha}}})\left(\frac{D}{\sigma}\right)^2$$

For the oscillatory motion of the vehicle to diminish, this factor should be negative or very small. It is pointed out in reference 1, however, that the relation between this factor and the dynamic stability breaks down at low speeds where the deceleration is appreciably modified by gravity. If the missile reaches a terminal speed at which the weight component along the flight path equals the drag, the dynamic stability is no longer a function of the drag. (Typical values of the above factor, including the drag term, become positive for the blunted cone where C_{L_α} has a large negative value and for the paraboloid where $C_{m_q} + C_{m_{\dot{\alpha}}}$ is small.) Various other simplifying assumptions are made in the analysis of reference 1 which did not have to be made in the simulation. In particular, the variation of C_D, C_{L_α}, and C_{m_α} with angles of attack and Mach number are ignored; the flight path is assumed to be unaffected by gravity; and density variations with altitude are simplified. The main assumption made in the simulation was that C_{m_q} varied only with Mach number as in figure 6.

Figure 11 presents the damping characteristic $1/T_{1/2}$ for several simulated flights of the blunted cone and the paraboloid. The deceleration is also shown because of its importance to dynamic stability. Of course, neither the damping nor the deceleration remains constant during a flight, so it was necessary to select a specific portion of the flight on which to base comparisons. Accordingly, the damping and deceleration shown in figure 11 and in succeeding figures were measured from the records for the first few cycles in the simulated flight.

Figure 11 shows that as the flight path was made more shallow and the deceleration became greater, the damping of the simulated missiles generally decreased. A lowering of the launch altitude also caused large increases in deceleration, but only the damping of the paraboloid was consistently reduced. Most of the remainder of the simulation was directed toward further isolating the various effects which contributed to these results. It should be stated that even in the marginal case of the paraboloid launched at 25,000 feet the perturbation eventually damped to a small value.

The effect of varying the initial angle-of-attack perturbation is shown in figure 12. Such effects were small despite the nonlinearity of the force and moment derivatives with angle of attack. This figure also shows that the effect of neglecting gravity was a large increase in deceleration and reduced damping. Typical trajectories and velocity histories associated with these flights are presented in figure 13. The

[redacted]

rapid initial decelerations without gravity which are associated with poor damping characteristics are apparent.

In order to isolate the effects of deceleration, simulated flights were made at a constant altitude of 40,000 feet with a fixed value of C_{m_q} of -0.05 with various rates of deceleration. The results are given in figure 14. The crosshatched area represents the range of values obtained as the initial angle-of-attack perturbation was varied from 0° to 40°. It can be seen that deceleration was always detrimental to the damping and can be considered the direct cause of at least part of the changes in damping shown in figure 11 to accompany deceleration.

The influence of C_{m_q} was next evaluated by simulated flights made with a fixed speed and altitude but with different values of C_{m_q}. The fixed speed condition is similar in effect to the terminal speed situation previously discussed and is not entirely unrealistic for the subsonic case. The aerodynamic characteristics affecting the damping were thus reduced to C_{L_α} and $C_{m_q} + C_{m_\alpha}$. Figure 15 shows the damping obtained when a C_{m_q} of 0 is assumed as compared to that when a C_{m_q} of -0.05 is used. A third assumption for the value C_{m_q} which is actually an attempt at conservative data extrapolation was suggested by the blunted-cone data in figure 5(a) at $M = 0.80$. For this case

$$C_{m_q} = 0.05 \qquad \text{for} \quad 0^\circ < \alpha < 4^\circ$$

and

$$C_{m_q} = 0 \qquad \text{for} \quad 4^\circ < \alpha < 40^\circ$$

Figure 15 shows that the damping is considerably reduced when the more conservative estimates of C_{m_q} are used. The importance of more complete experimental damping data in an investigation of this type is apparent. In the previous simulated flights, the assumed values of C_{m_q} approached 0 only in the case of the paraboloid flying at a Mach number near 0.7. It appears probable that the effects of deceleration included an effect due to decreasing C_{m_q} for this flight.

Figure 16 shows that at 40,000 feet altitude a negative value of C_{m_q} was not even required for neutral stability of the paraboloid if there was no deceleration. The blunted cone was not quite as good in this respect because of the unfavorable C_{L_α} it exhibited at large angles of attack.

The force and moment variations with angle of attack that were included in the simulation also affected the frequency of the oscillation.

[redacted]

Figure 17 presents the frequency as a function of the initial angle-of-attack perturbation for simulated flights at fixed speed and altitude. The variation of frequency was, of course, largest for the blunted cone because of its large change in C_{m_α} near 16° angle of attack.

The flights in two degrees of freedom (velocity and altitude constant) were also convenient for determining how the force and moment characteristics at various Mach numbers affected the dynamic responses. The value of C_{m_q} was assumed to be -0.05 for these flights. Figure 18 shows the results for a range of angle-of-attack perturbations. The damping characteristics appear to be only moderately affected by Mach number when C_{m_q} is fixed.

CONCLUDING REMARKS

The aerodynamic characteristics of two blunt bodies at subsonic speeds have been determined in wind-tunnel tests. The damping-in-pitch derivative, when measured about moment centers ahead of the maximum diameter, was negative for both bodies except at small angles of oscillation. The model with a parabolic forebody had a lower drag coefficient, a more positive lift-curve slope, a more nearly linear pitching-moment variation with angle of attack, and generally less damping in pitch than the model with a blunted-cone forebody. Removal of the afterbodies decreased the drag, increased the lift-curve slope, and increased the damping of the models. Base pressures were approximately 40 percent of the dynamic pressure below the free-stream static pressure.

The test results were applied to an analog-computer study of the dynamics of two representative missiles. A broad range of flight conditions was considered in the study, including angle-of-attack perturbations up to 40°, flight-path angles from 20° to 60° below the horizontal, and altitudes from 25,000 to 65,000 feet. The bodies were dynamically stable for most of the simulated conditions. Limitations in the wind-tunnel data left doubt as to the stability of the bodies at large angles of oscillation. The simulated trajectory and velocity history of one of the bodies were closely checked by those of a model actually dropped from 40,000 feet altitude.

Ames Research Center
National Aeronautics and Space Administration
Moffett Field, Calif., Mar. 2, 1959

[redacted]

REFERENCES

1. Allen, H. Julian: Motion of a Ballistic Missile Angularly Misaligned With the Flight Path Upon Entering the Atmosphere and Its Effect Upon Aerodynamic Heating, Aerodynamic Loads, and Miss Distance. NACA TN 4048, 1957. (Supersedes NACA RM A56F15)

2. Bird, John D., and Reese, David E., Jr.: Stability of Ballistic Reentry Bodies. NACA RM L58E02a, 1958.

3. Short, Barbara J., and Sommer, Simon C.: Some Measurements of the Dynamic and Static Stability of Two Blunt-Nosed, Low-Fineness-Ratio Bodies of Revolution in Free Flight at $M = 4$. NASA TM X-20, 1959.

4. Beam, Benjamin H.: A Wind-Tunnel Test Technique for Measuring the Dynamic Rotary Stability Derivatives at Subsonic and Supersonic Speeds. NACA Rep. 1258, 1956. (Supersedes NACA TN 3347)

5. Herriot, John G.: Blockage Corrections for Three-Dimensional-Flow Closed Throat Wind Tunnels With Consideration of the Effect of Compressibility. NACA Rep. 995, 1950. (Supersedes NACA RM A7B28)

6. Den Hartog, J. P.: Mechanical Vibrations, McGraw-Hill Book Co., Inc., 1940, p. 470.

[redacted]

TABLE I.- DATA ON FREE-FALL MODELS

Forebody	Paraboloid	Blunted cone
Length, ft	1.408	1.175
Maximum diameter, ft	1.500	1.500
Distance from nose to c.g., ft	.515	.375
Mass, slugs	8.600	6.690
Moment of inertia, slug-ft^2	1.425	.765

[redacted]

[redacted]

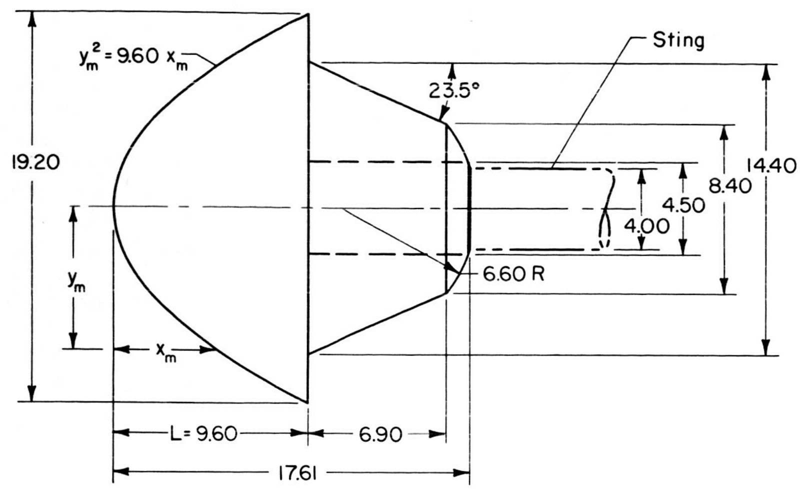

Paraboloid

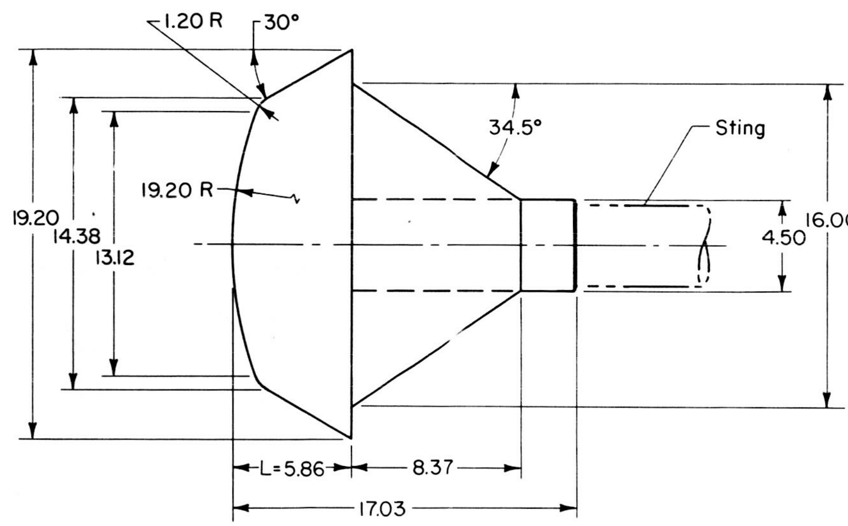

Large Blunted Cone

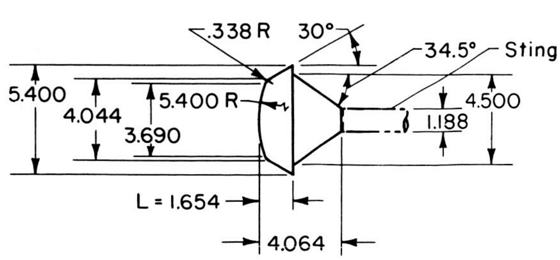

All dimensions in inches unless noted otherwise

Small Blunted Cone

(a) Model dimensions.

Figure 1.- The wind-tunnel models.

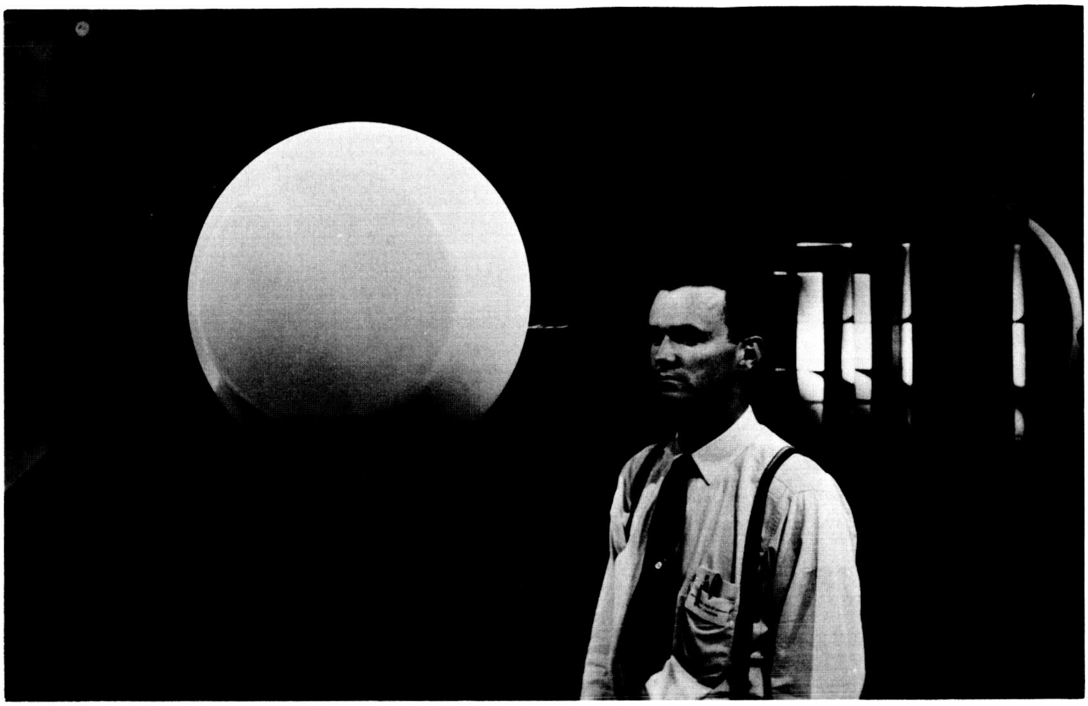

A-22159

A-22160

(b) Model mounted in the wind tunnel.

Figure 1.- Concluded.

[redacted]

All dimensions in inches unless noted otherwise

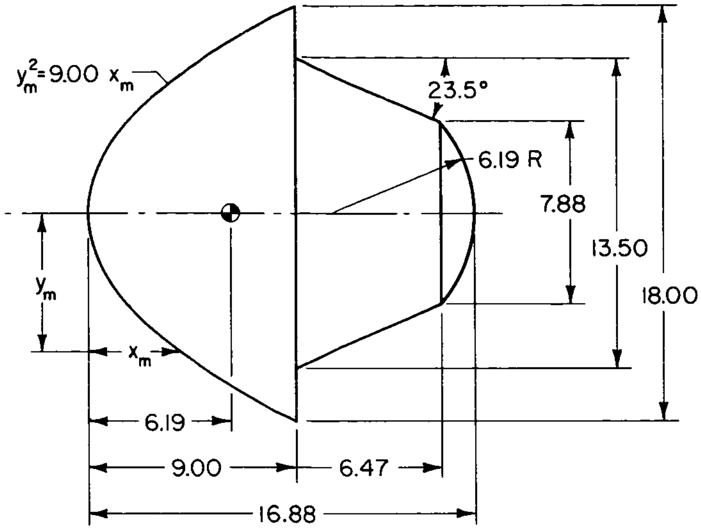

Paraboloid

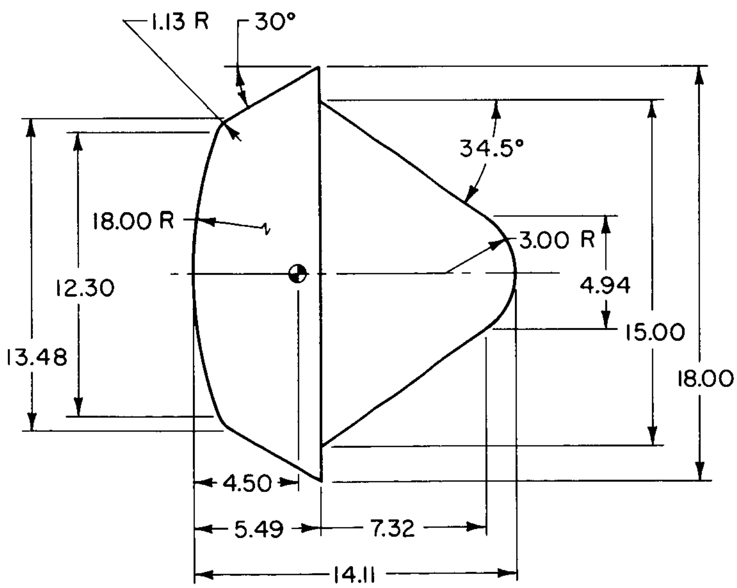

Blunted Cone

(a) Model dimensions.

Figure 2.- The free-fall models.

[redacted]

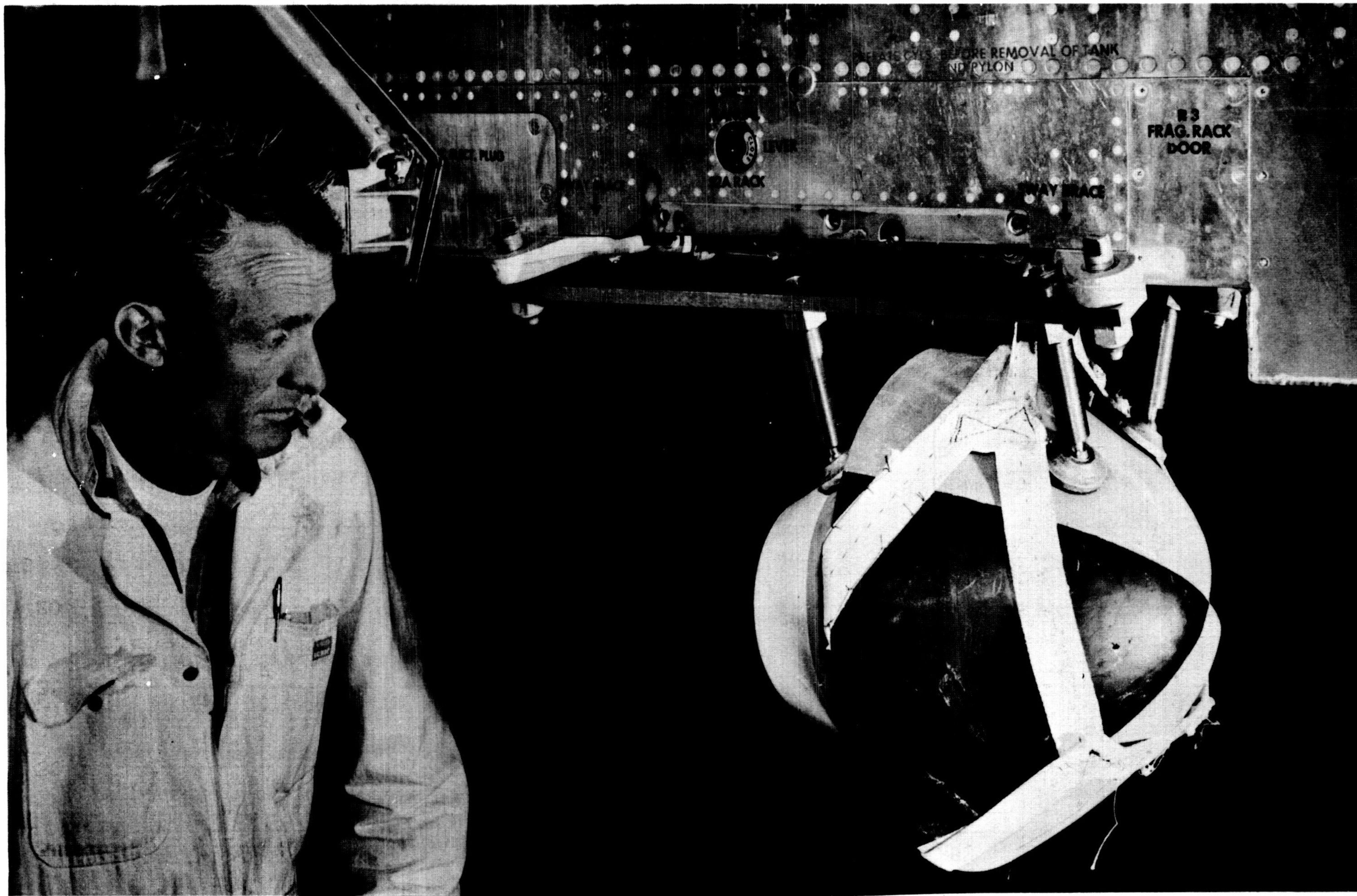

A-21910

(b) Model mounted on the drop airplane.

Figure 2.- Concluded.

[redacted]

[redacted]

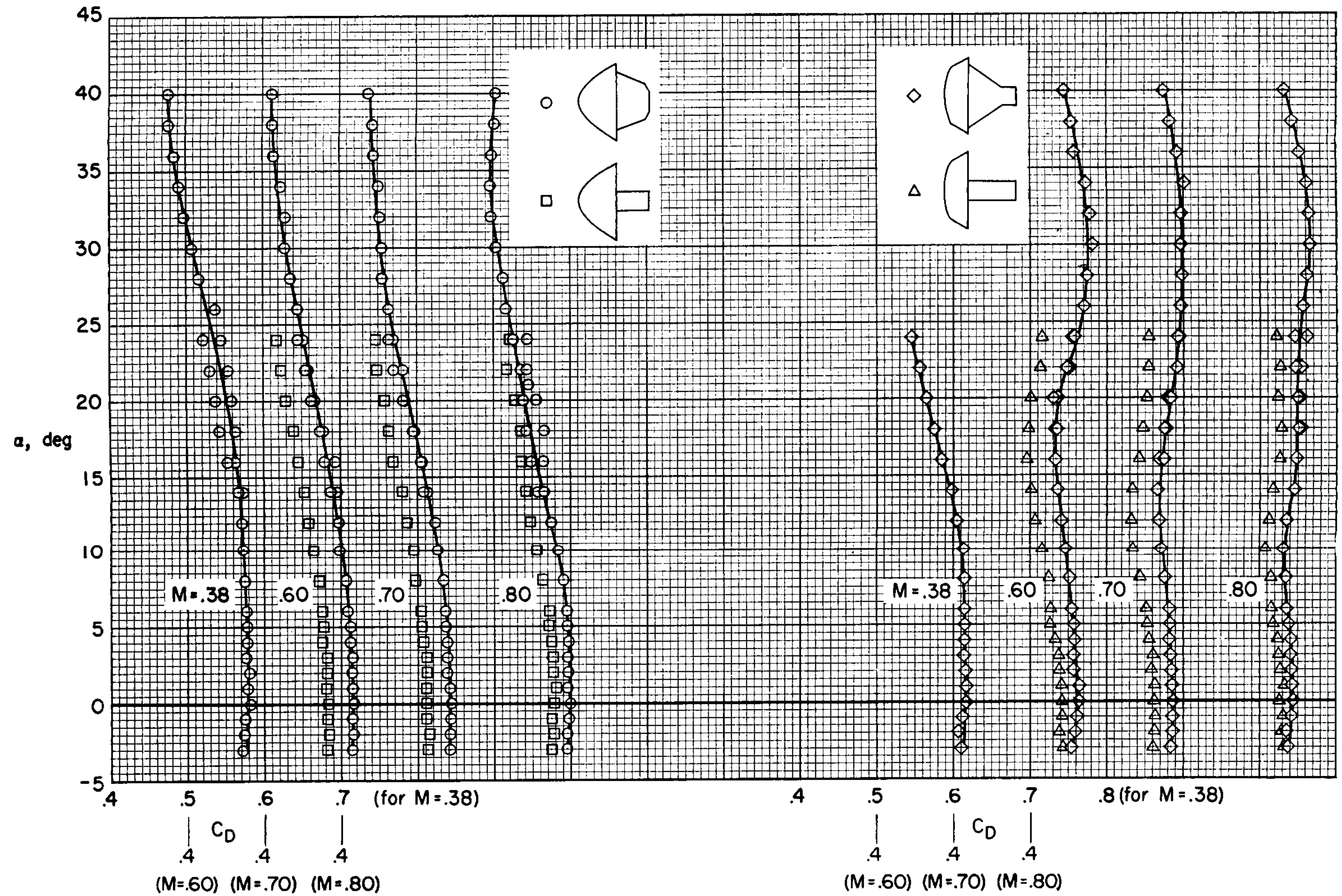

(a) Drag.

Figure 3.- Static force and moment characteristics of the models; maximum diameter = 1.6 feet, R $\geq$ 3 million.

[redacted]

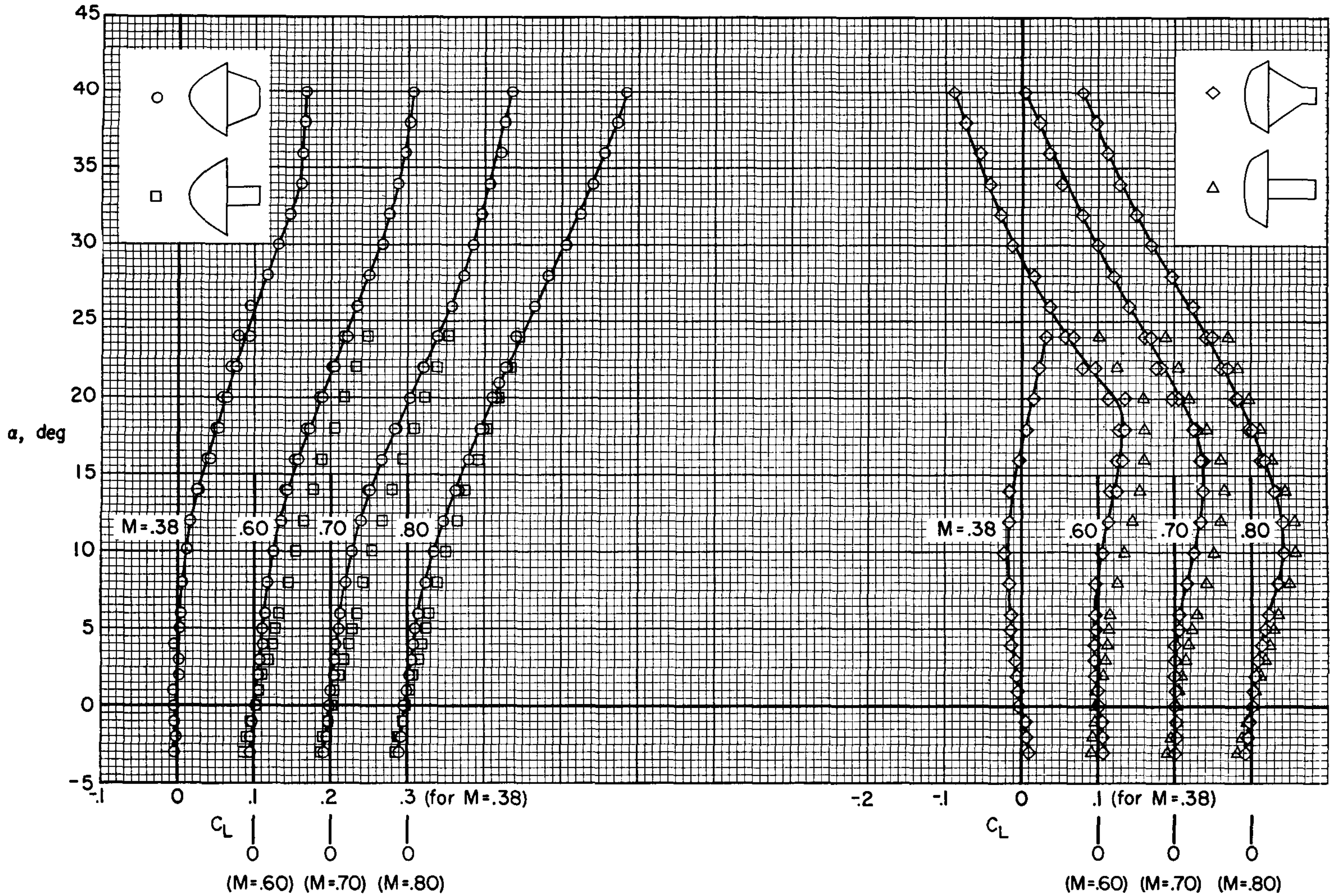

(b) Lift.

Figure 3.- Continued.

[redacted]

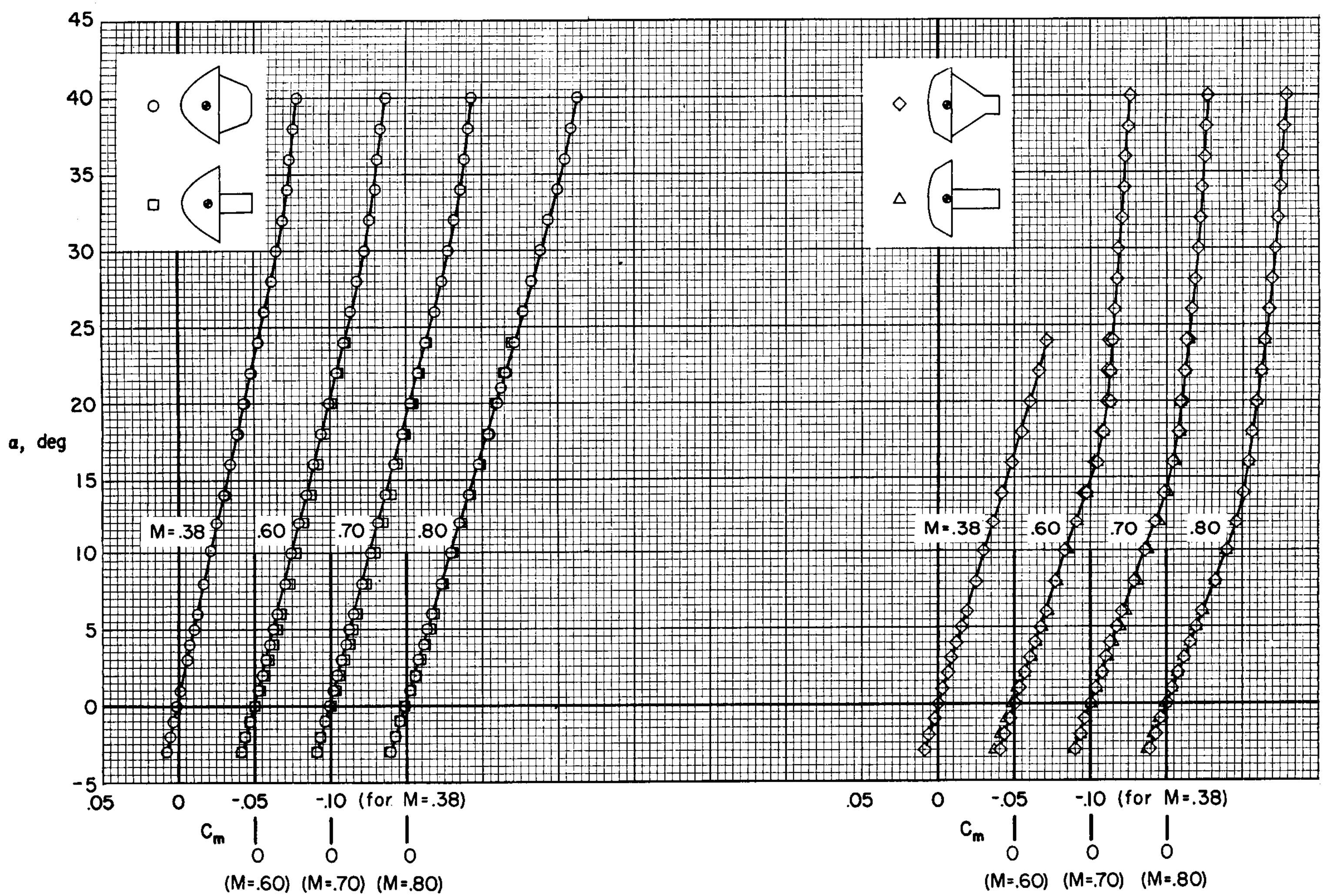

(c) Pitching moment.

Figure 3.- Concluded.

[redacted]

[redacted]

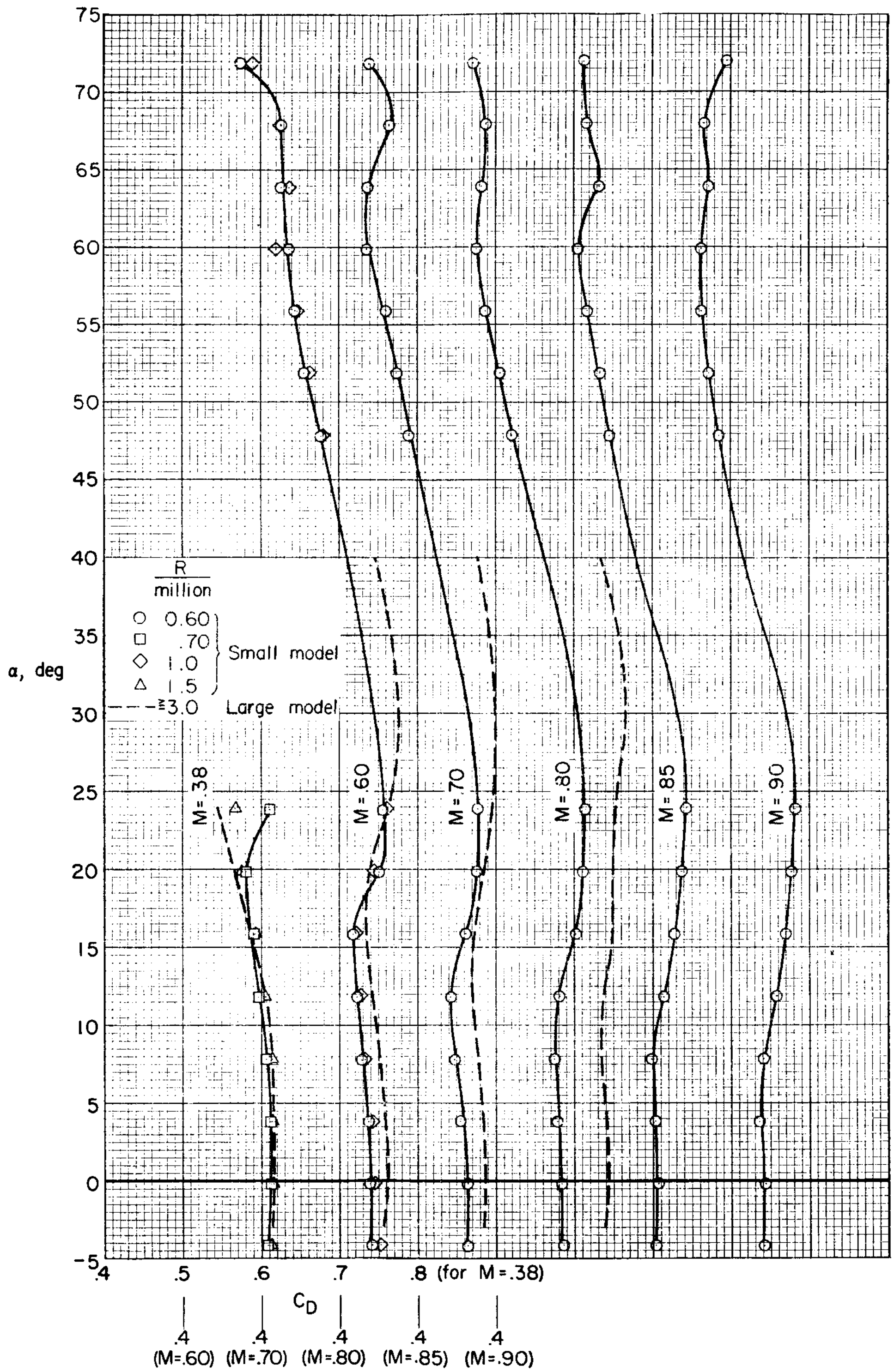

(a) Drag.

Figure 4.- Comparison of static force and moment characteristics of the blunted-cone models.

[redacted]

[redacted]

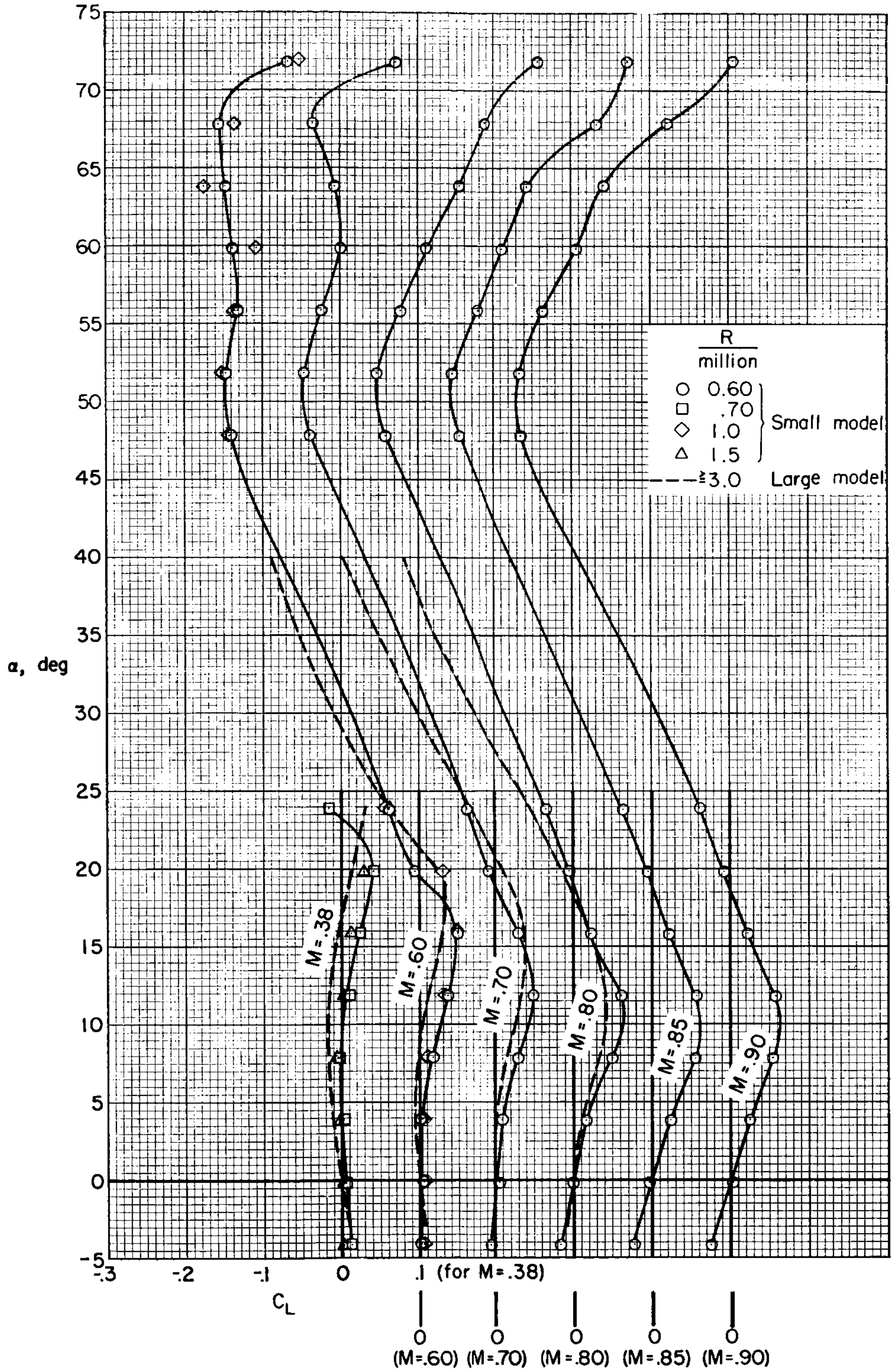

(b) Lift.

Figure 4.- Continued.

[redacted]

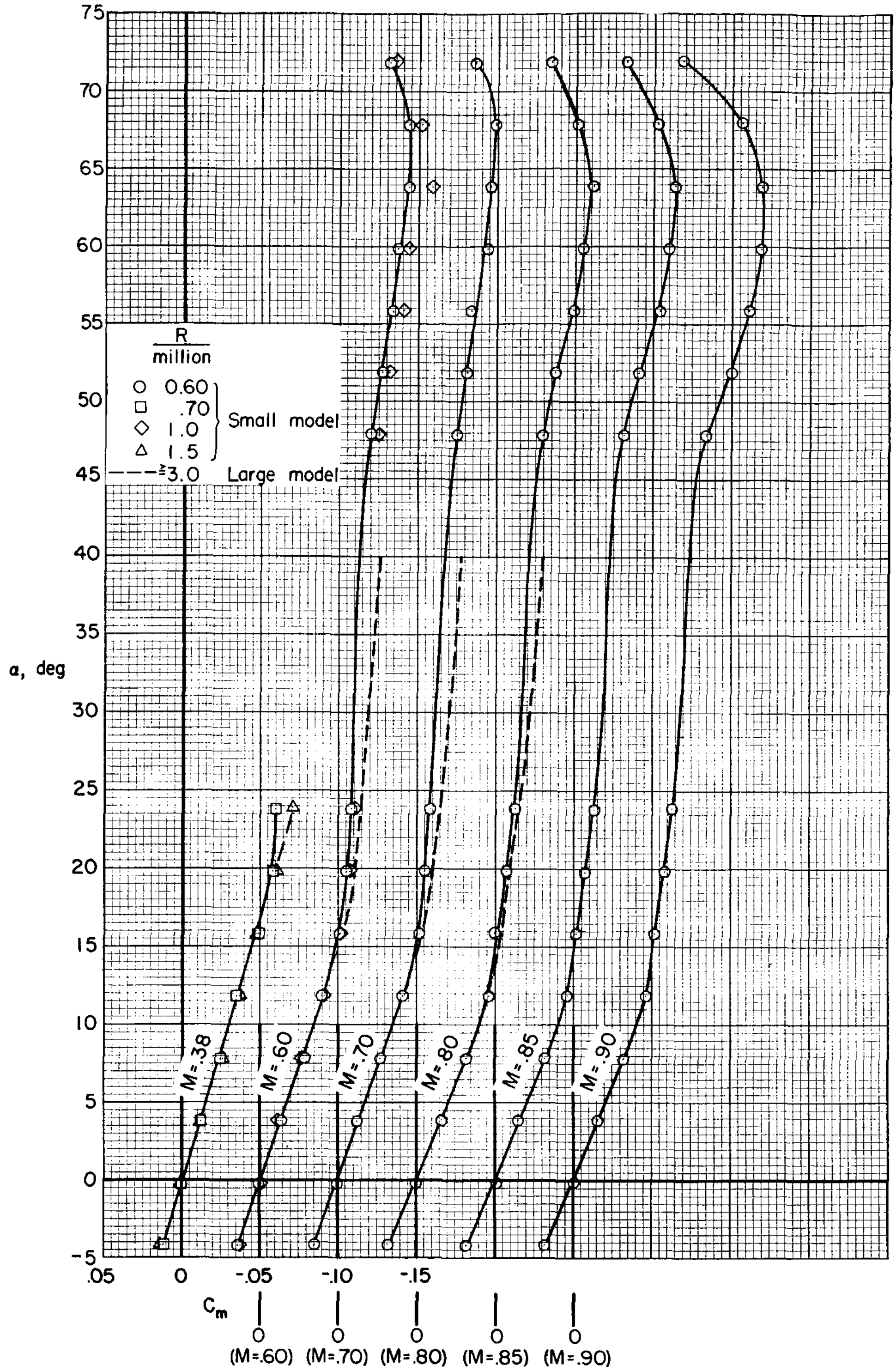

(c) Pitching moment.

Figure 4.- Concluded.

[redacted]

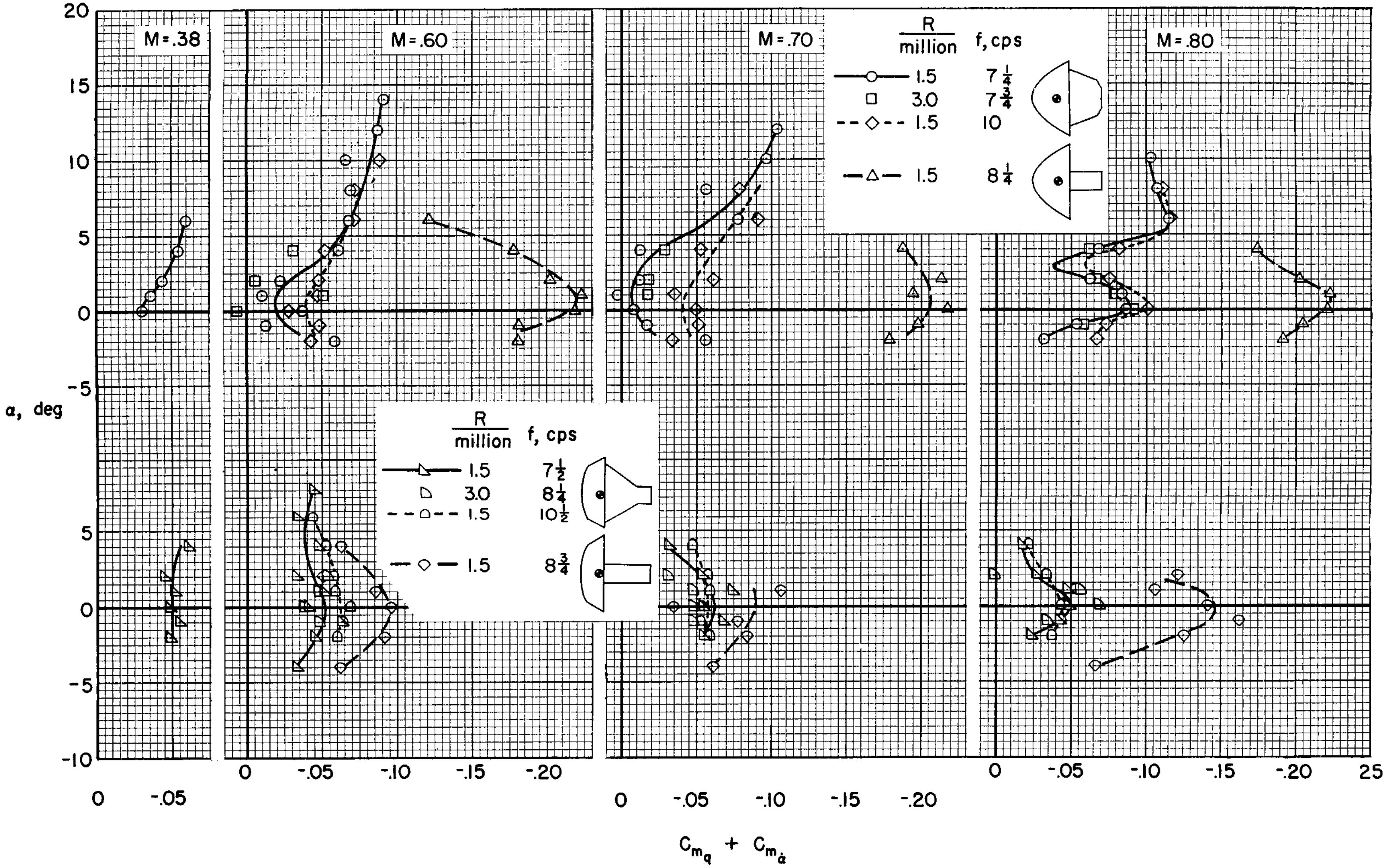

(a) Effects of Reynolds number, oscillation frequency, and afterbody.

Figure 5.- The aerodynamic damping coefficients of the models.

[redacted]

[redacted]

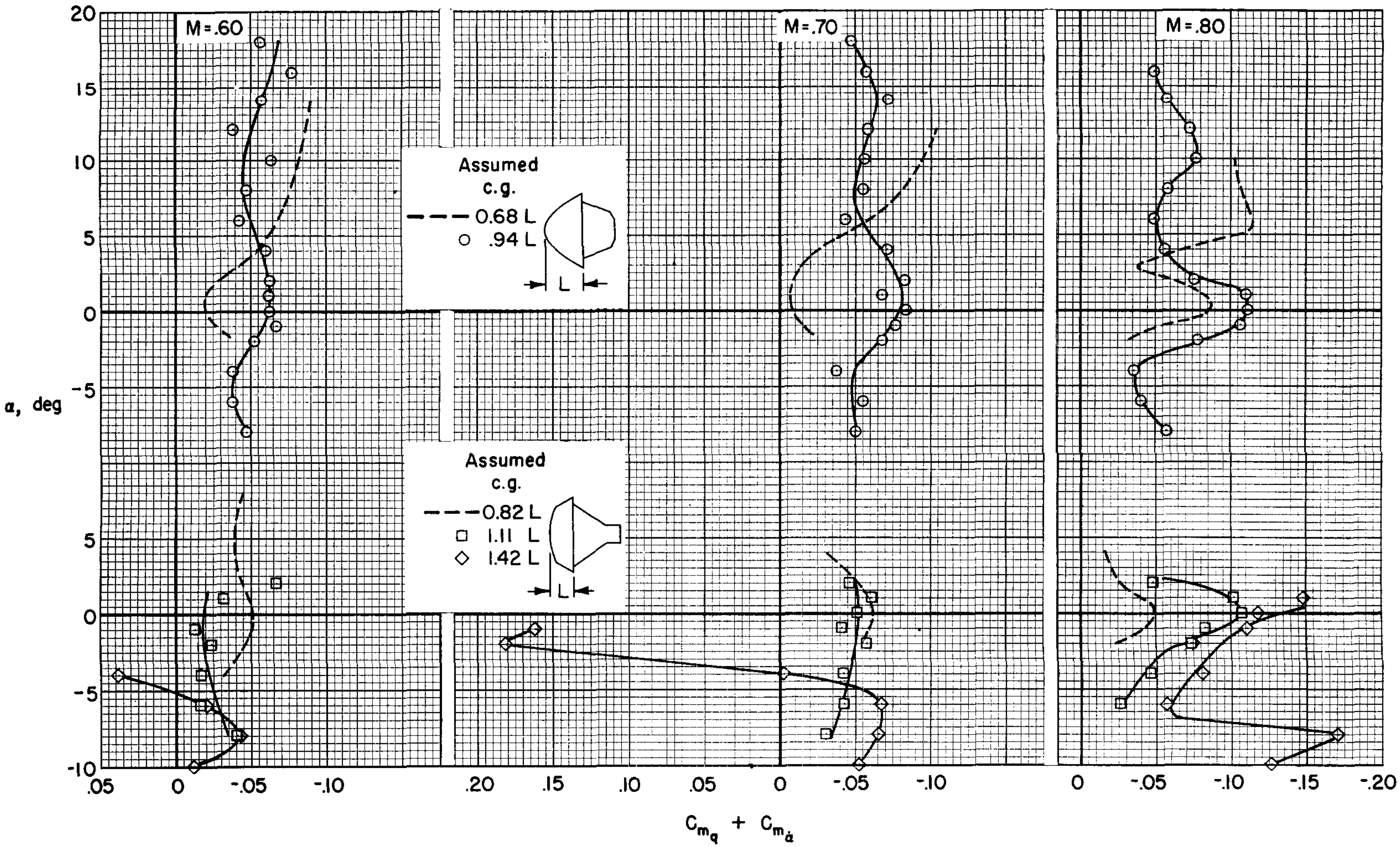

(b) Effects of center of rotation (assumed c.g.); R = 1.5 million, f ≈ 7 cps.

Figure 5.- Concluded.

[redacted]

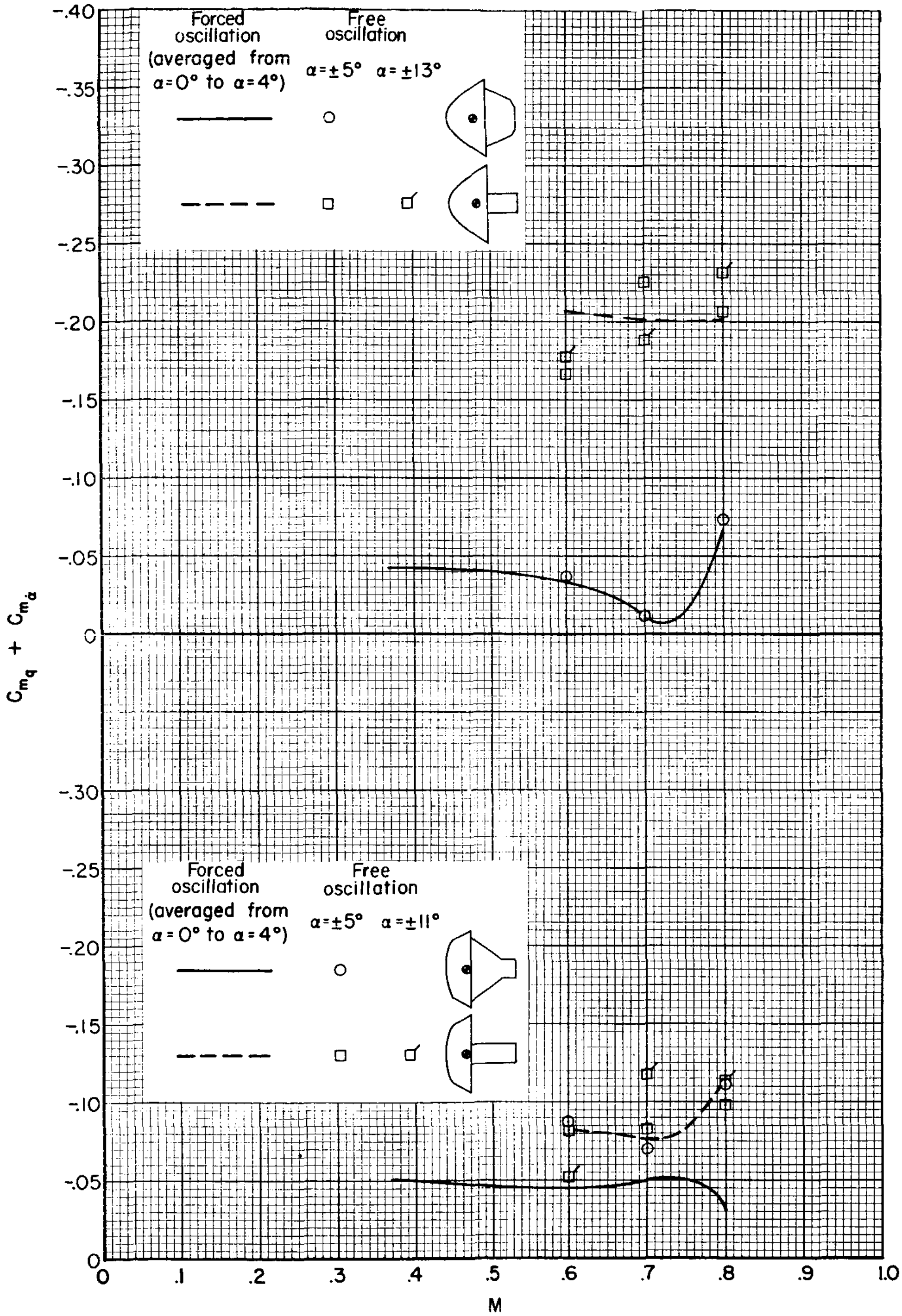

Figure 6.- A comparison of damping measured on the forced-oscillation mechanism with that determined from movies of free oscillations of the models; R = 1.5 million, frequency for free oscillations about 1/2 frequency for forced oscillations.

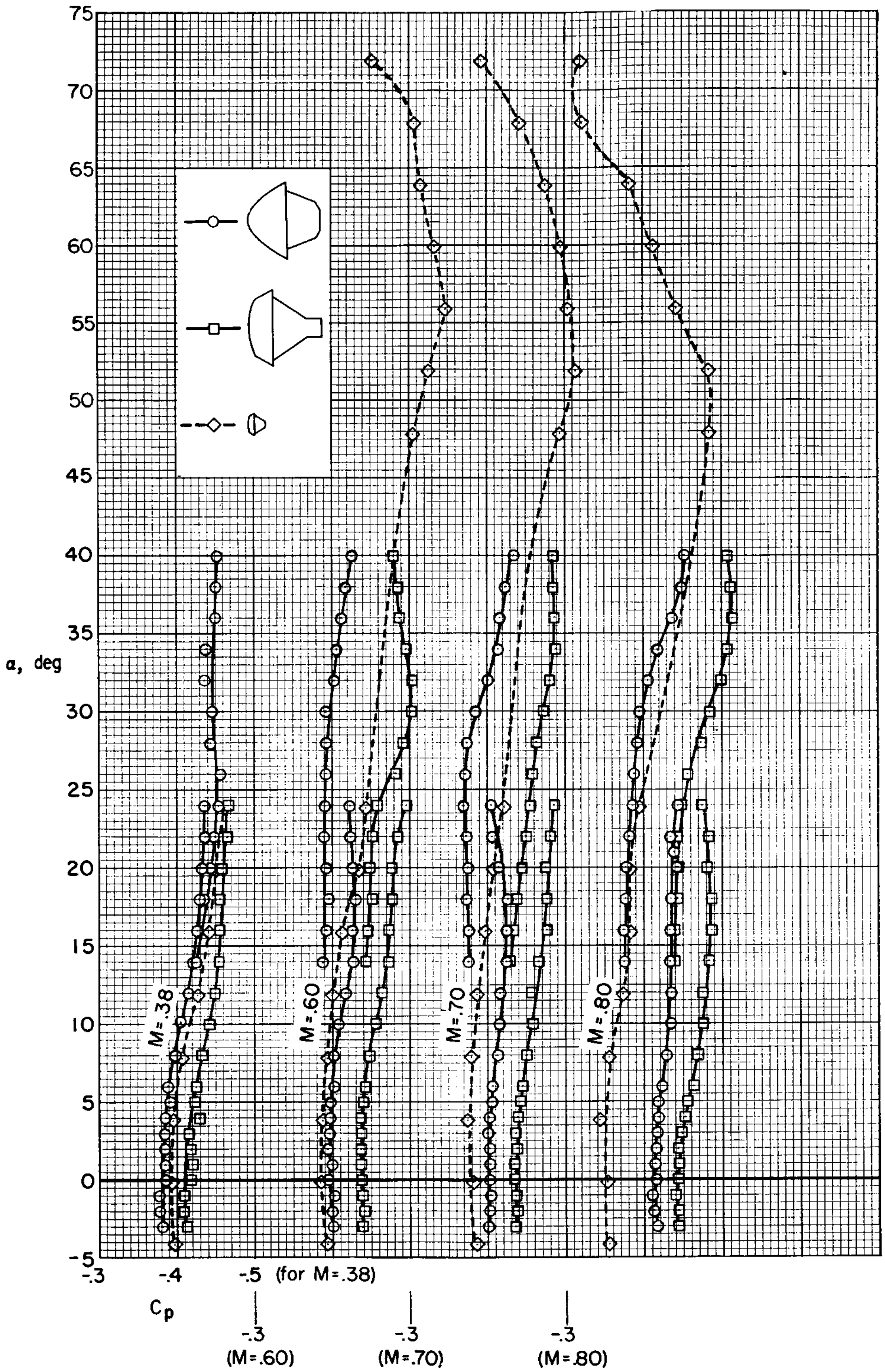

Figure 7.- Pressure coefficients at the base of the models; R for large models ≥ 3 million, R for small models ≤ 0.7 million.

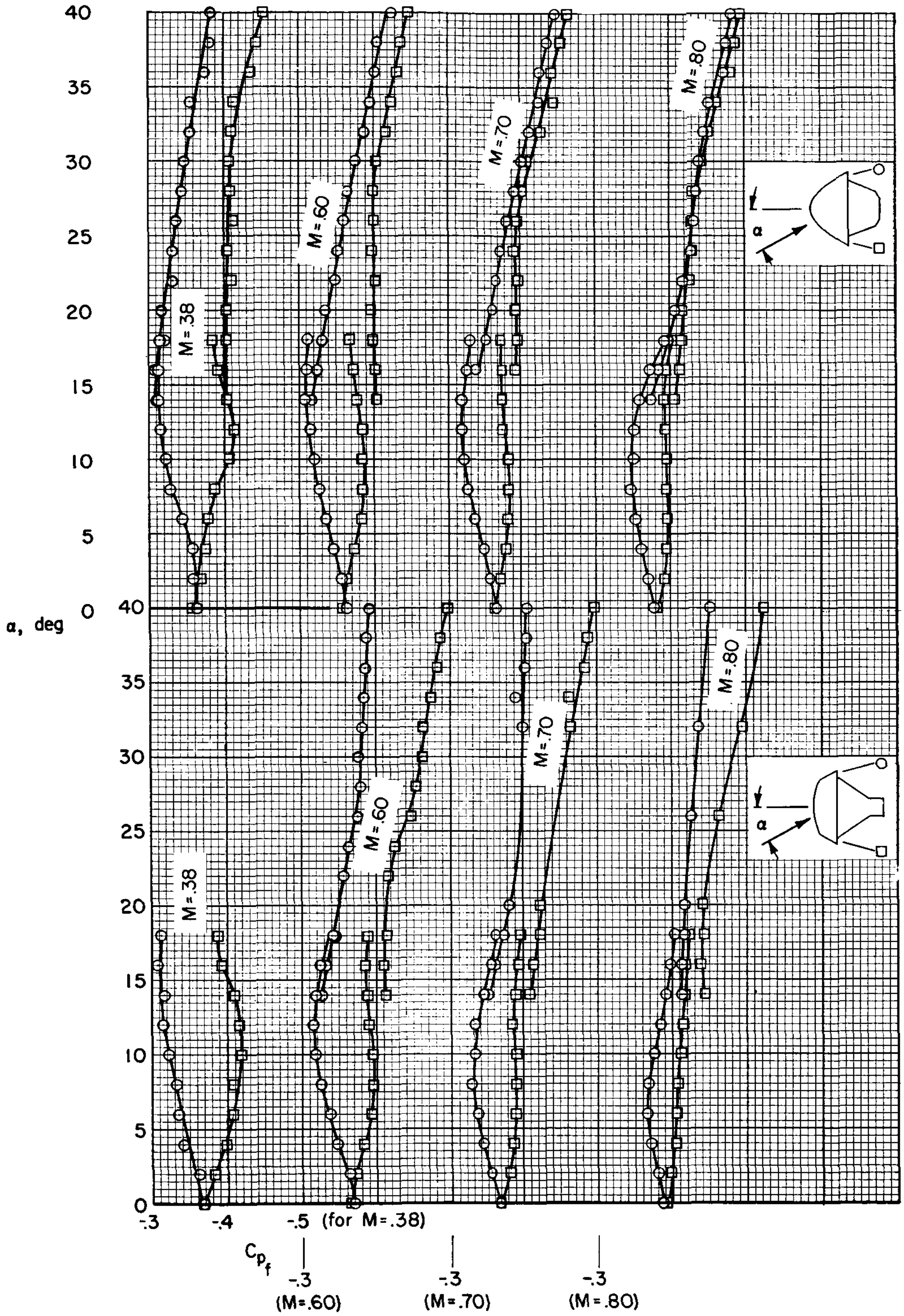

Figure 8.- Pressure coefficients at the base of the forebodies; R ≥ 3 million.

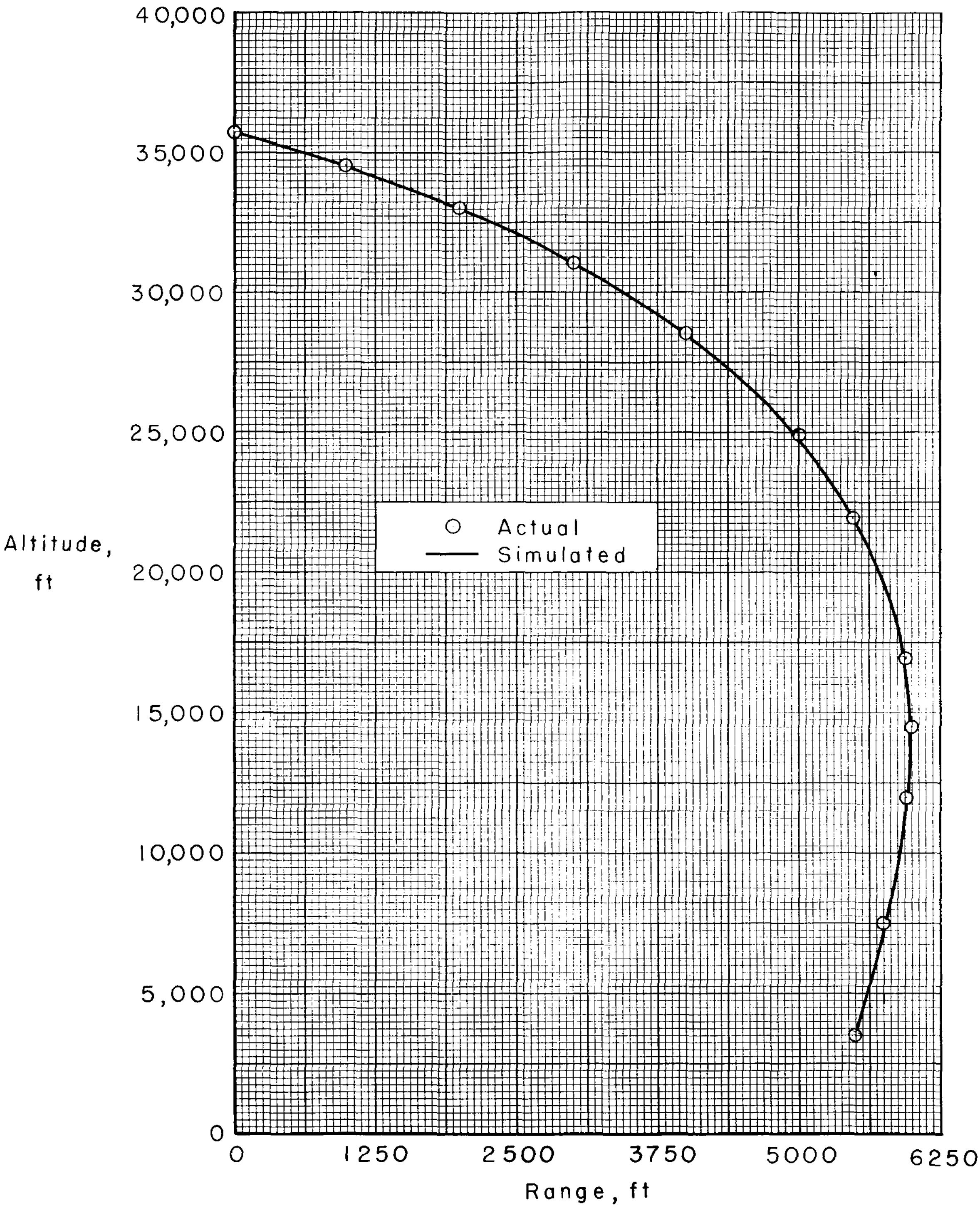

Figure 9.- Comparison of actual and simulated trajectories for the blunted cone.

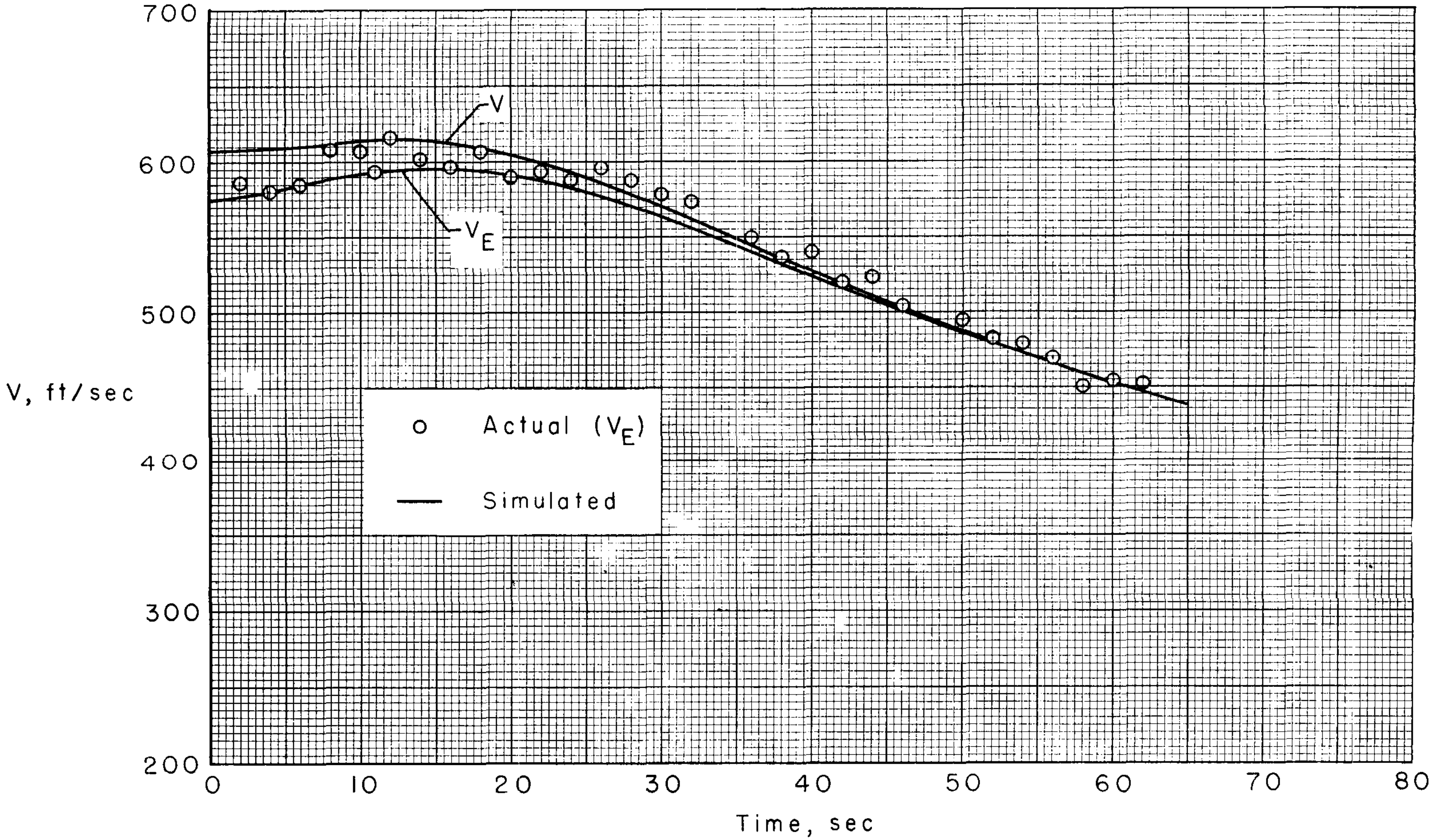

Figure 10.- Comparison of actual and simulated flight velocities for blunted cone relative to air (V) and relative to the earth (V_E).

[redacted]

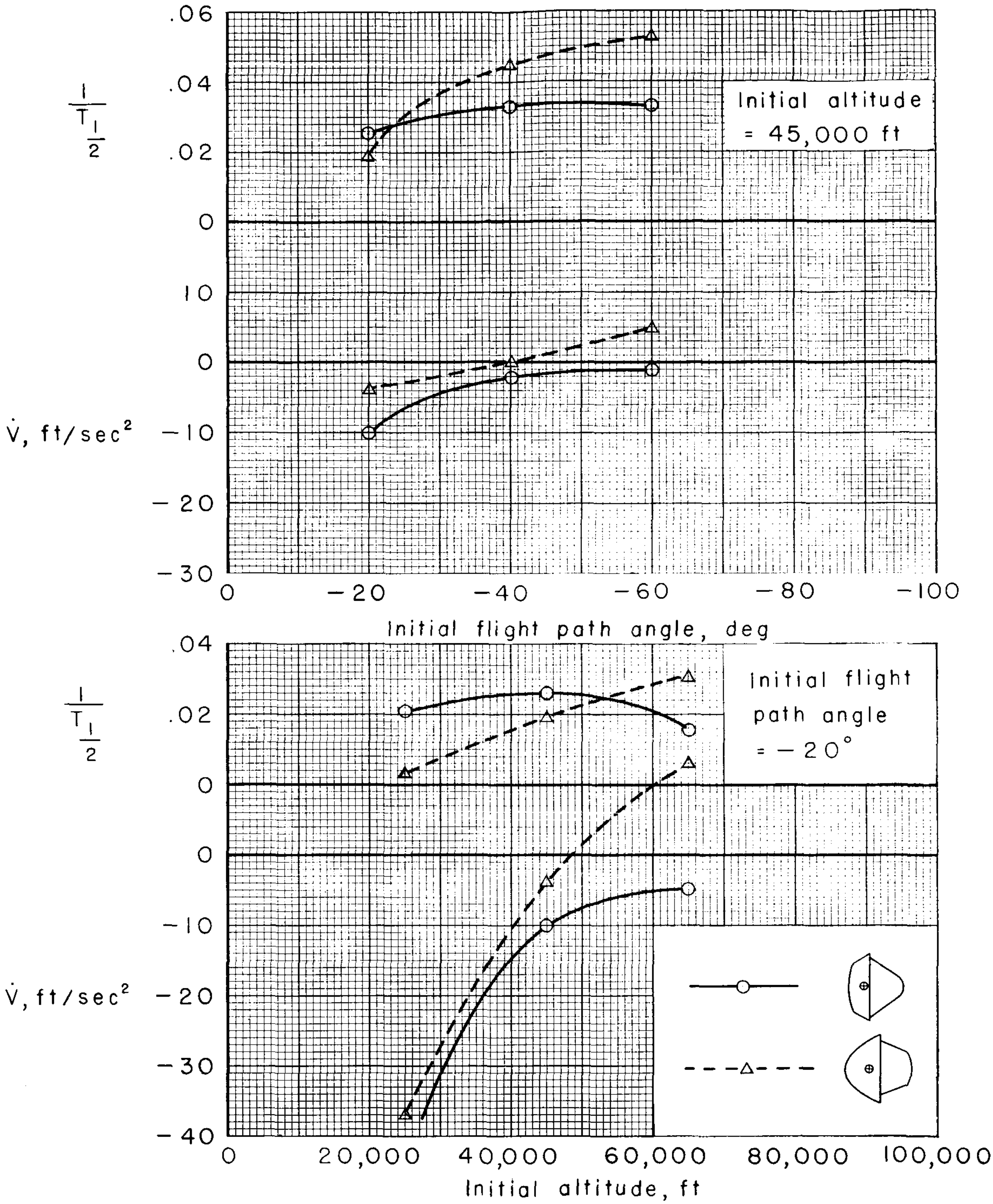

Figure 11.- The damping characteristics and deceleration for simulated flights launched with angle-of-attack perturbation of 40° and Mach number of 0.80.

[redacted]

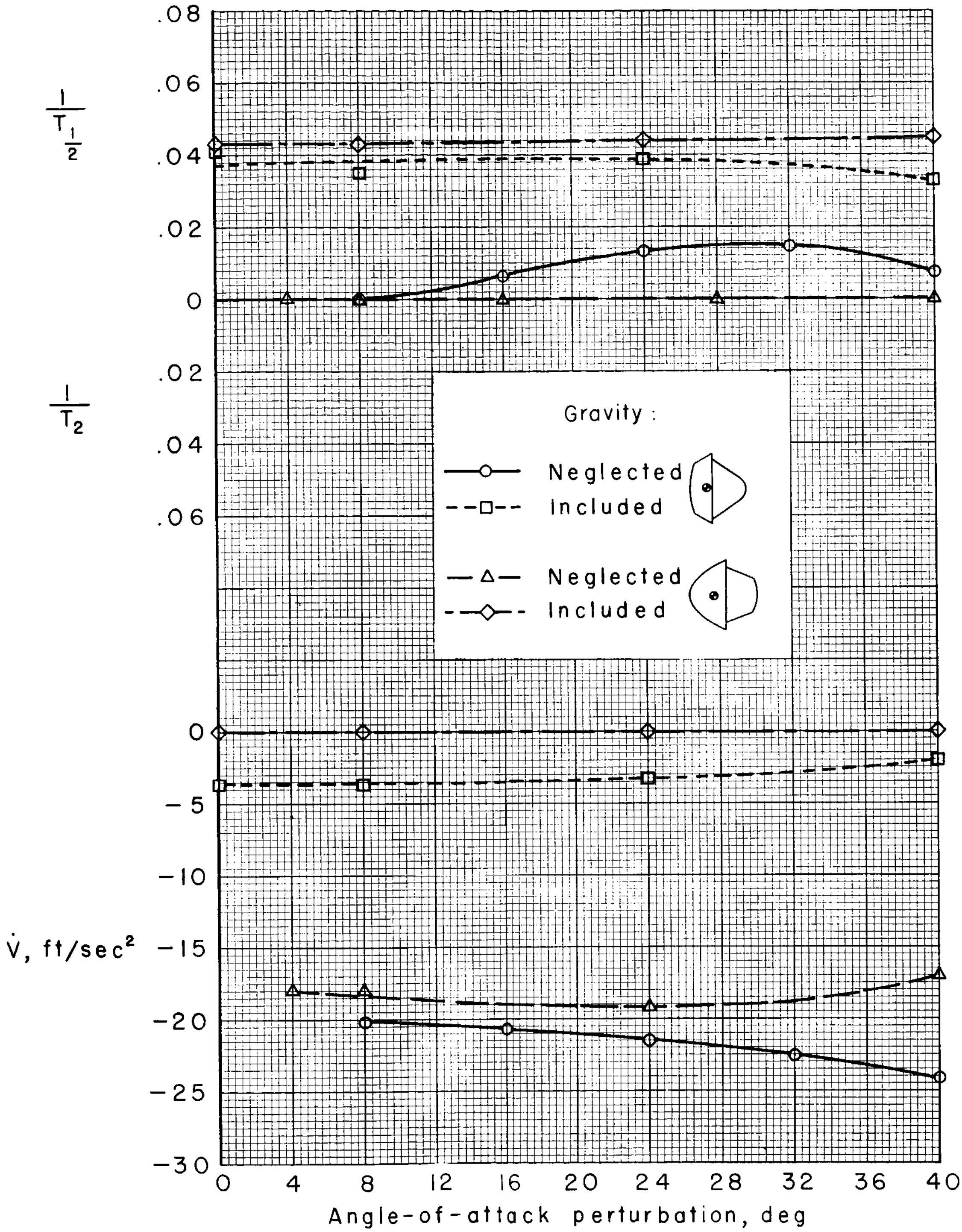

Figure 12.- The damping characteristics and deceleration with and without the effect of gravity for simulated flights launched at altitude of 45,000 feet, flight path angle of -40°, and Mach number of 0.80.

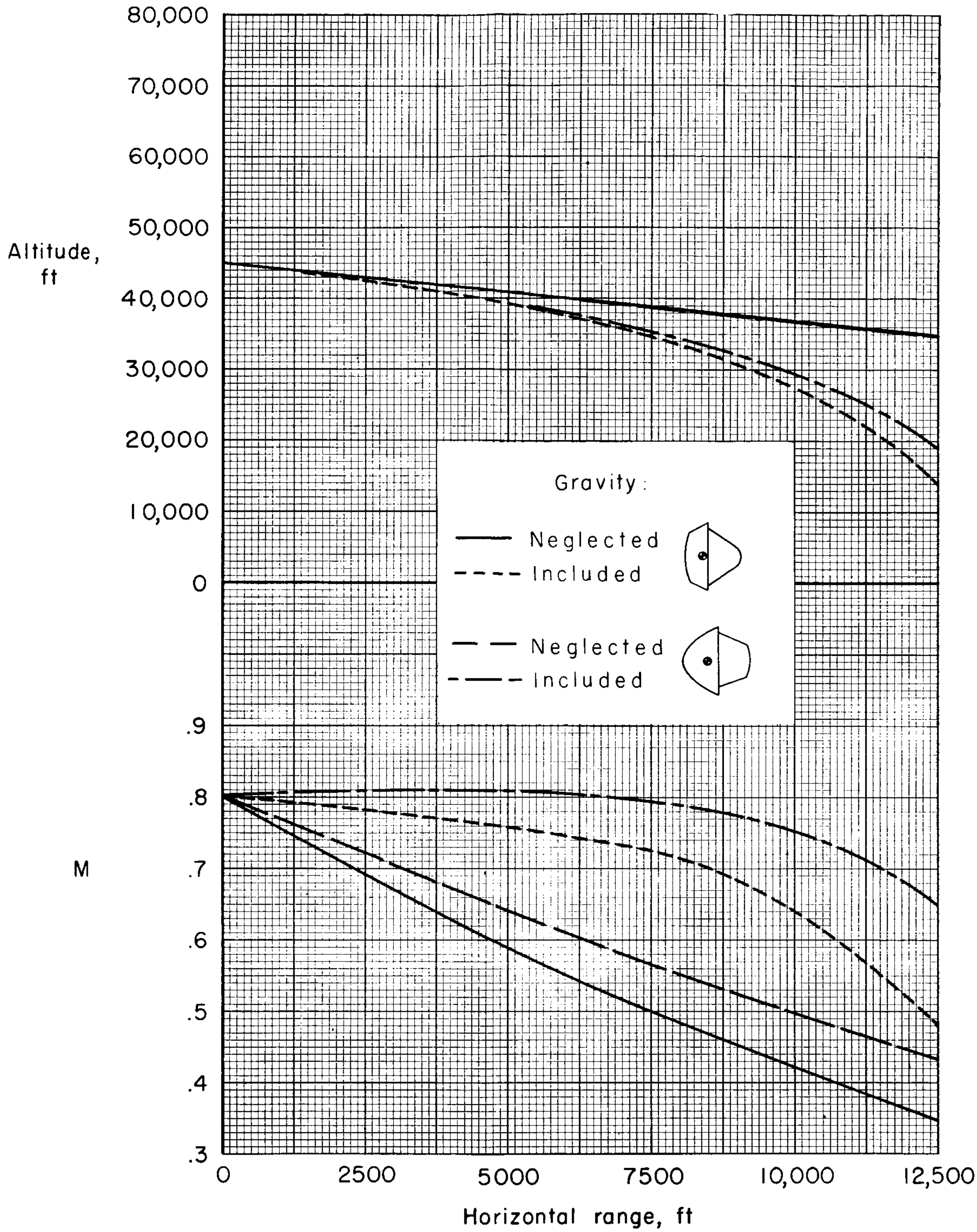

Figure 13.- The trajectories for simulated flights launched at altitude of 45,000 feet and flight path angle of -40° with and without the effects of gravity.

[redacted]

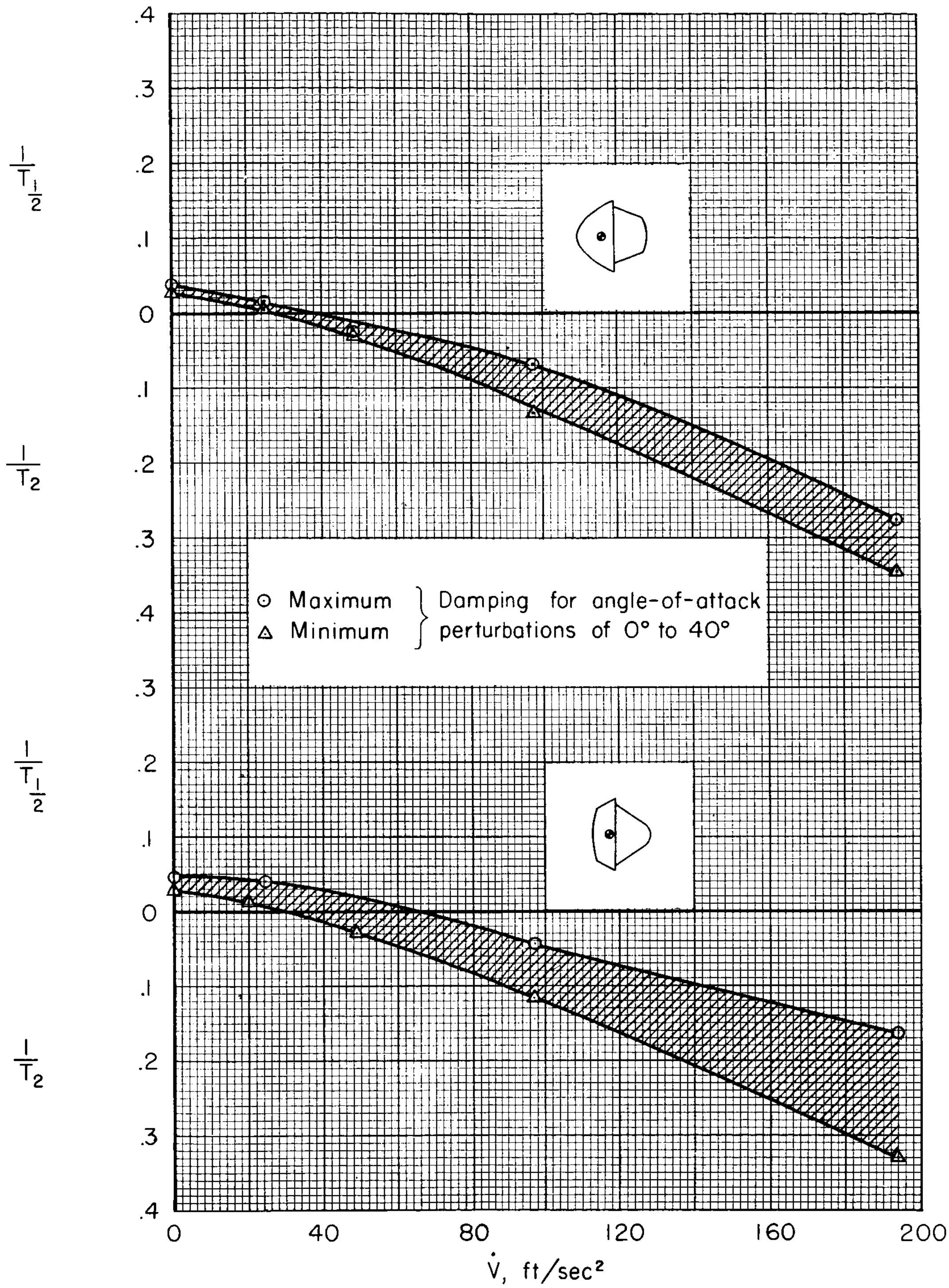

Figure 14.- The variation of damping with longitudinal deceleration for simulated flights at a constant altitude of 40,000 feet; C_{m_q} fixed at -0.05, flights launched at Mach number of 0.8.

[redacted]

[redacted]

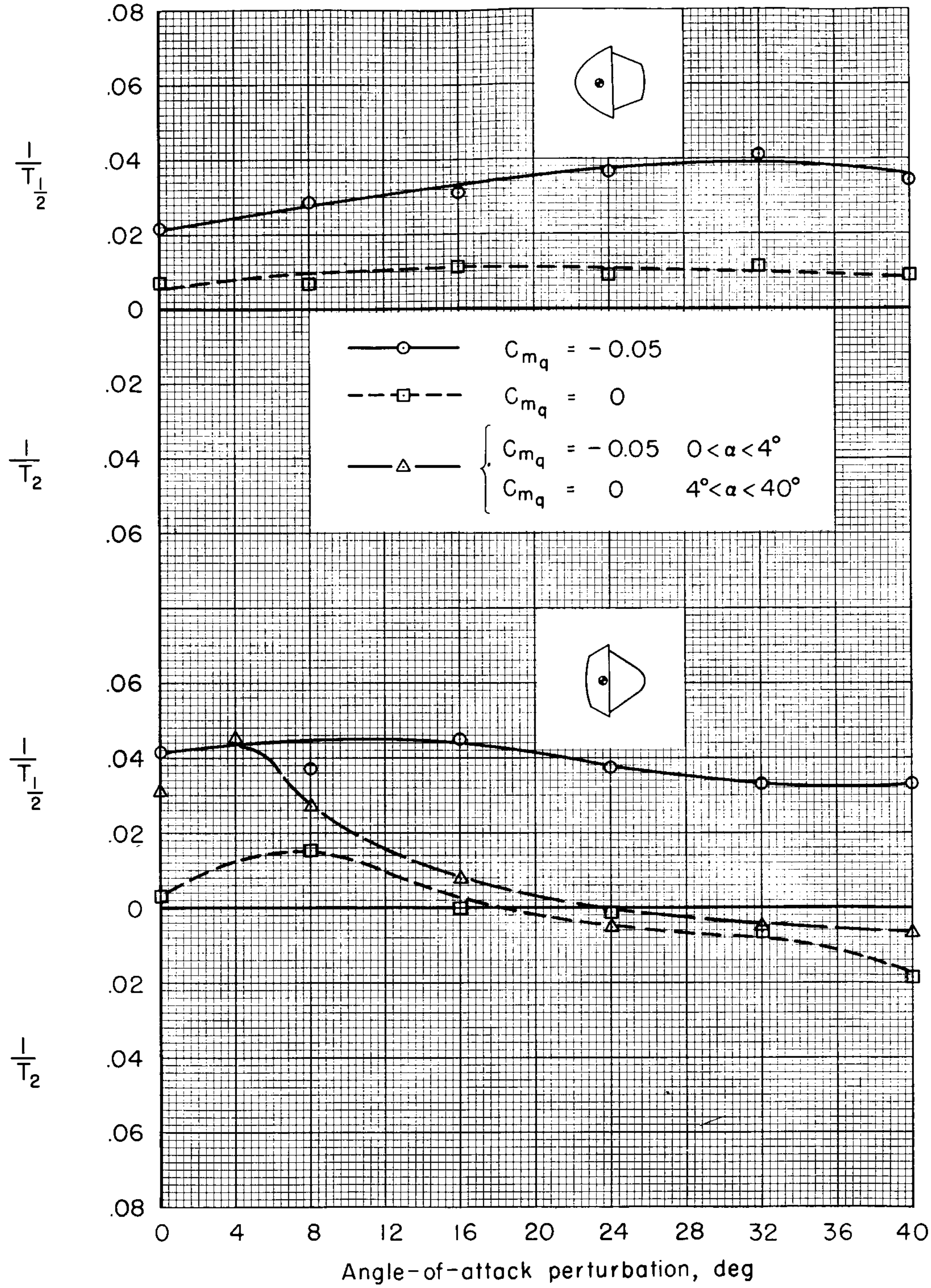

Figure 15.- The effect of C_{m_q} on the damping characteristics of the simulated missiles flying at a constant Mach number of 0.80 at a constant altitude of 40,000 feet.

[redacted]

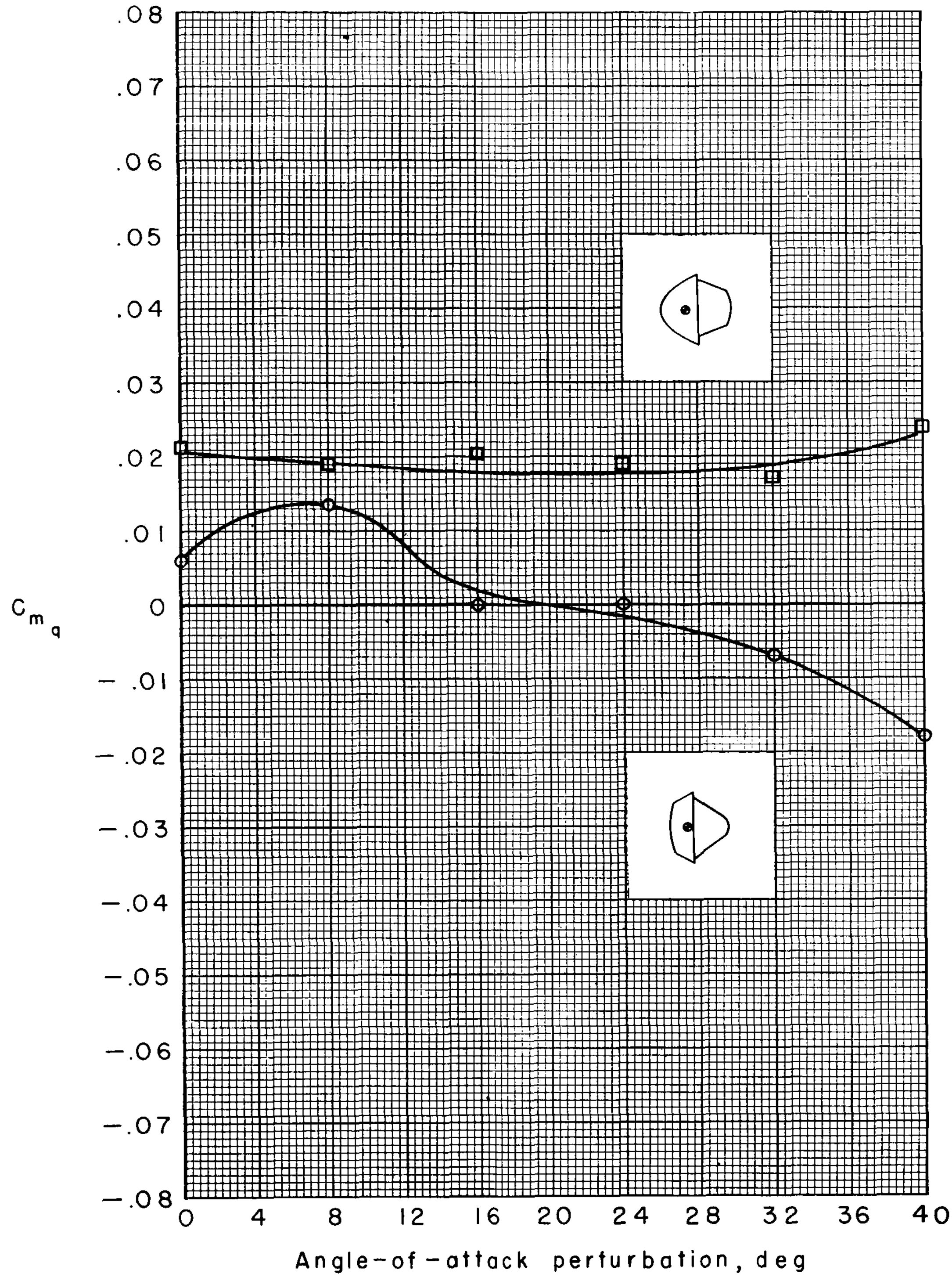

Figure 16.- The value of C_{m_q} required for neutral stability of the simulated missiles flying at a constant Mach number of 0.8 at a constant altitude of 40,000 feet.

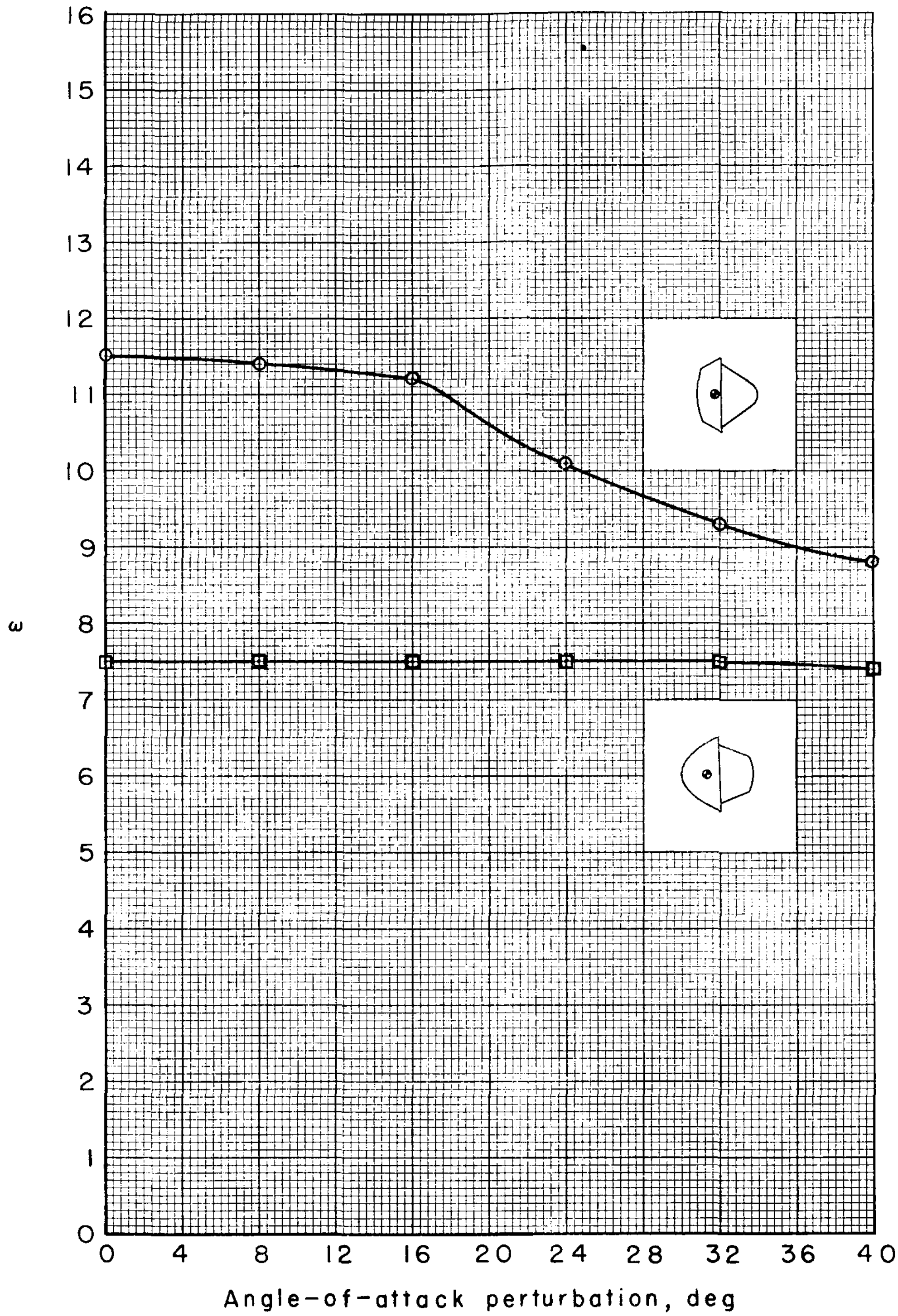

Figure 17.- The frequency of oscillation of the simulated missiles flying at a constant Mach number of 0.8 at a constant altitude of 40,000 feet; $C_{m_q} = -0.05$.

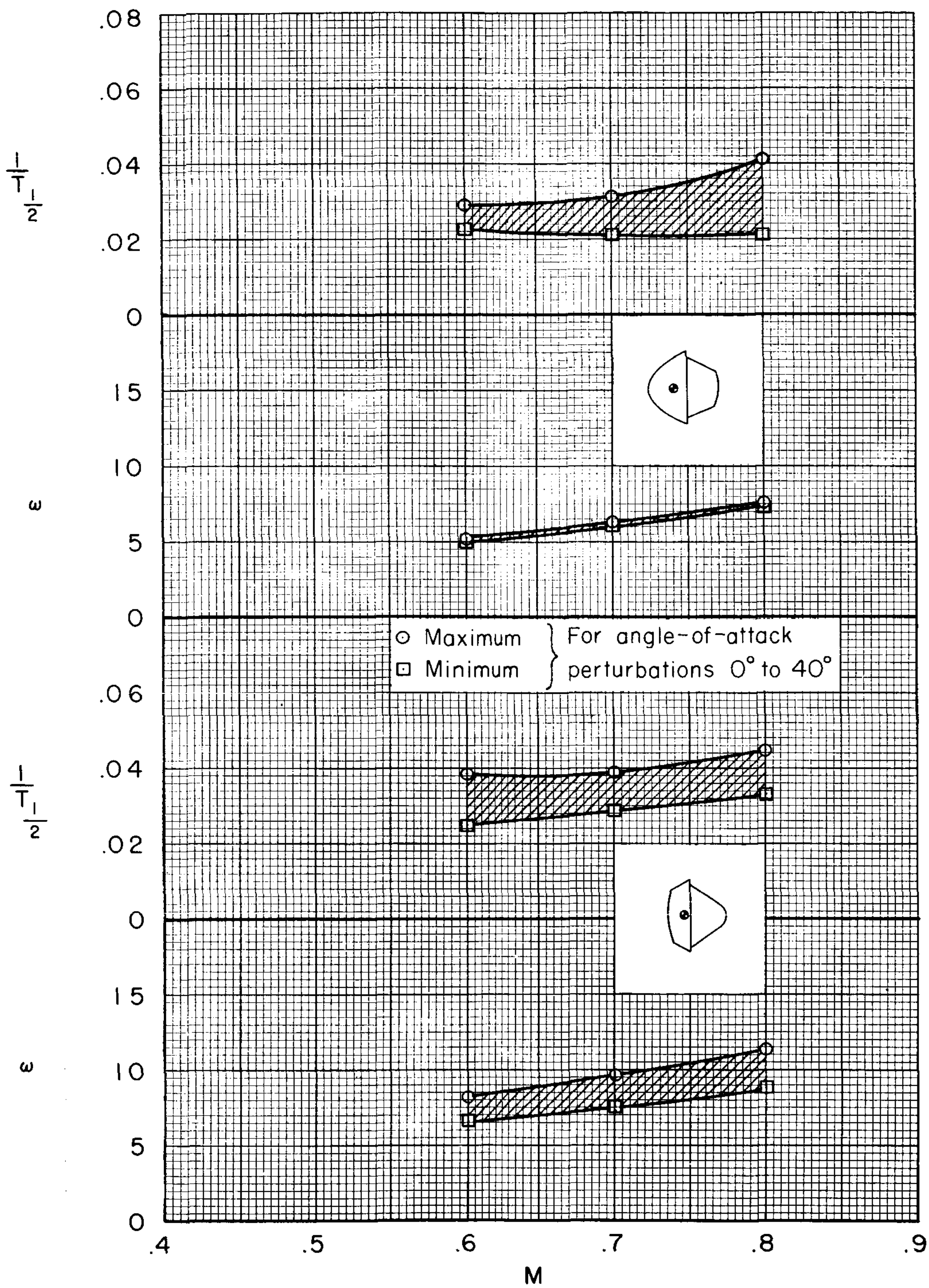

Figure 18.- The damping and frequency characteristics of the simulated missiles flying at various Mach numbers with no deceleration at a constant altitude of 40,000 feet; $C_{m_q} = -0.05$.